COMPARATIVE EVALUATION OF THE MICROGAP OF PREMACHINED TITANIUM AND ZIRCONIA ABUTMENTS AT THE IMPLANT-ABUTMENT INTERFACE BEFORE AND AFTER CYCLIC LOADING –AN IN VITRO STUDY

Dissertation Submitted to

THE TAMILNADU DR. M.G.R. MEDICAL UNIVERSITY

In partial fulfillment for the Degree of

MASTER OF DENTAL SURGERY

BRANCH I

PROSTHODONTICS AND CROWN & BRIDGE

APRIL 2012

CERTIFICATE

This is to certify that the dissertation titled **"COMPARATIVE EVALUATION OF THE MICROGAP OF PREMACHINED TITANIUM AND ZIRCONIA ABUTMENTS AT THE IMPLANT-ABUTMENT INTERFACE BEFORE AND AFTER CYCLIC LOADING –AN IN VITRO STUDY"** is a bonafide record work done by **Dr. SUDHARSHAN RAMACHANDRAN** under our guidance and to our satisfaction during his post graduate study period between 2009 – 2012.

This dissertation is submitted to **THE TAMILNADU DR. M.G.R. MEDICAL UNIVERSITY**, in partial fulfillment for the Degree of **MASTER OF DENTAL SURGERY – PROSTHODONTICS AND CROWN & BRIDGE, BRANCH I.** It has not been submitted (partial or full) for the award of any other degree or diploma.

Guided by

RAGAS DENTAL COLLEGE & HOSPITAL CHENNAI

Dr. N.S. Azhagarasan, M.D.S.,
Professor and Head of the Department,
Department of Prosthodontics
and Crown & Bridge,
Ragas Dental College & Hospital
Chennai

PROFESSOR & HEAD
DEPT OF PROSTHODONTICS
Ragas Dental College & Hospital
Chennai - 600 113.

Dr. S. Ramachandran, M.D.S.,
Principal,
Ragas Dental College & Hospital
Chennai

PRINCIPAL
RAGAS DENTAL COLLEGE & HOSPITAL

ACKNOWLEDGEMENT

This dissertation is the result of work with immense support from many people and it is a pleasure now that I have the opportunity to express my gratitude to all of them.

I would be failing in my duty if I do not adequately convey my heartfelt gratitude and my sincere thanks to my Head of the Department, ***Professor Dr. N.S. Azhagarasan, M.D.S.,*** *Department of Prosthodontics and Crown & Bridge, Ragas Dental College and Hospital, Chennai, for his exceptional guidance, tremendous encouragement, well-timed suggestions and heartfelt support throughout my postgraduate programme which has never failed to drive the best out of me. I would like to profoundly thank him for giving an ultimate sculpt to this study. I will remember his help for ages.*

I wish to express my gratitude to ***Dr. S. Ramachandran, M.D.S., Principal,*** *Ragas Dental College and Hospital, Chennai, for his encouragement throughout my postgraduate course. I also thank him for permitting me to make use of the amenities in the institution.*

I would like to express my real sense of respect, gratitude and thanks to my ***Professor Dr. K. Chitra Shankar M.D.S.,*** *for her guidance, constant support, back up and valuable criticism extended to me during the period of my study. The timely help and encouragement rendered by her had been enormously helpful throughout the period of my postgraduate study.*

I would also like to thank ***Dr. K. Madhusudan, M.D.S., Dr.S.Jayakrishnakumar, M.D.S., Dr.Manoj Rajan, M.D.S., Dr. Saket Miglani, M.D.S., Dr. K. Manikandan, M.D.S., Dr. M.Saravana Kumar, M.D.S., Dr. Vallabh Mahadevan, M.D.S., Dr. Sabarinathan. M.D.S., Dr. Divya, Krishnan, M.D.S.,*** *for their valuable suggestions and help given throughout my study.*

I would like to solemnly thank ***Dr. R. Hariharan, M.D.S., Senior Lecturer,*** *for the valuable guidance and encouragement rendered by him. This dissertation has been the fertile outcome of his massive endurance, support, proficient guidance and counsel.*

I would also like to thank ***Mr. C. V. Krishnakumar*** *for his invaluable help, guidance and encouragement in designing and executing the custom-made cyclic loading machine and* ***Mr. Lokesh*** *for his technical expertise.*

I would like to like to express my gratitude to ***Dr. Saphal Shetty*** *for his help in supplying the components used in this study.*

I would also like to thank ***Dept. of Manufacturing Engineering, Anna University,*** *Chennai for extending their support and expertise in the measurement phase of my study.*

I thank ***Ms. R. Deepa,*** *Statistician, Ragas Dental College and Hospital for helping me with the statistical analysis for the study.*

*It would not be justifiable on my part if I do not acknowledge the help of my **fellow colleagues, seniors and juniors** for their criticism and continuous support throughout my postgraduate course.*

*I wish to thank **my sister, brother in-law, nephew and fiancé** for their moral support, care and encouragement in all walks of my life.*

*Last but not the least, even though words wouldn't do much justice, I would like to specially thank my parents **Dr. S. Ramachandran and Dr. Sudha S. Ramachandran** for their blessings and love.*

Above all I thank GOD almighty for all the grace endowed upon me.

CONTENTS

LIST OF TABLES

ANNEXURE

LIST OF FIGURES

Fig.9c: Mixing spiral

Fig.9d: Automixing gun

Fig.10: Die lubricant

Fig.11: Inlay casting wax

Fig.12: PKT instruments

Fig.13a: Sprue wax

Fig.13b: Surfactant spray

Fig.13c: Investment ring and crucible former

Fig.13d: Phosphate bonded investment material

Fig.13e: Colloidal silica

Fig.13f: Carborundum separating discs

Fig.13g: Ni-Cr alloy pellets

Fig.14: Aluminum oxide powder – 110 μm

Fig.15a: Tungsten carbide metal trimming burs

Fig.15b: Silicon carbide rubber points

Fig.16: Resin-modified glass ionomer cement

Fig.17a: Agate plastic spatula

Fig.17b: Plastic instrument

Fig.17c: Hand scaler

Fig.17d: Mixing pad

Fig.18: Custom-made jig

Fig.19: Dental surveyor

LIST OF GRAPHS

INTRODUCTION

Dental implantology has revolutionized the treatment for edentulous and partially edentulous patients, and successful implant integration has been well documented.[47] The use of dental implants to support and retain dental prostheses has been demonstrated to be clinically efficacious.[32] Implant-supported prostheses have been found to be an effective treatment alternative offering promising results for the replacement of missing teeth. Clinical evidence has shown excellent long-term results for osseointegrated implants with success rate above 90%.[3, 61] The biological, esthetic, and functional results were found to be good to excellent. [26]

The success of the implant-supported restoration is assessed by implant mobility, peri-implant radiolucency, vertical bone loss, absence of symptoms such as pain and infections and esthetic outcome.[3] Peri-implant radiolucency demonstrates the quantity and quality of bone surrounding the implant. Successful implant therapy requires dynamic equilibrium between mechanical, biologic and esthetic factors.[20] Mechanical factors, such as the implant-abutment precise fit, abutment screw preload, passive fit of prosthesis, occlusal forces, crown-to-implant ratio and type of restorative material used are involved in the success of implant rehabilitation.[48] Biological factors like the bone surrounding the implant, gingival health and osseointegration have been reported to influence implant therapy.[9, 40]

An implant-supported rehabilitation is comprised by an endosseous implant that is connected to a transmucosal abutment (2-piece), which receives the single or multiple unit prosthetic restorations.[34] The connection between the implant and the abutment is known as implant-abutment interface. The implant-abutment interface in butt-joint connections reveals a microgap.[22, 33] The implant-abutment connection can be an area where adverse mechanical and biological complications can occur.[34] Mechanical complications include increased incidences of abutment rotation and breakage,[14,17] screw loosening,[4, 12] and preload reduction.[34] Increased microleakage, gingivitis, and bone loss are the biological complications that have been reported from poorly adapted implant-abutment interface.[34]

One of the important mechanical factors that prevent abutment screw loosening and fracture is screw joint preload. It is defined as the tension generated in an abutment screw upon tightening and is a direct determinant of clamping force.[56] The preload loss during the occlusal load with the prosthesis in function favors the misfit of the implant-abutment connection and this can result in stress increase in the implant and connection components,[2, 6, 60] and consequently in the surrounding bone, which can also cause screw fracture and loss, abutment and prosthesis damage.[9, 20, 28, 48] Abutment to implant contact is important in the reduction of loading on abutment and prosthesis retaining screws, and thus help to ensure the maximum effectiveness of these

components.[17] Loading forces on implants may also contribute to the bacterial colonization of the implant-abutment microgap.[52]

Biologic complications such as increased microleakage, [29, 50] gingivitis, and bone loss [30, 45] have been reported with poorly adapted (misfit) implant-abutment interface.[9, 34] Microgaps at the implant-abutment interface allow microorganisms to penetrate and colonize the inner part of the implant and peri-implant soft tissues, leading to peri-implantitis, progressive bone loss and eventually implant loss.[29, 48] The abutment-implant interface plays an important role in order to maintain the integrity of the peri-implant bone, which is considered as one of the factors for the success of implant therapy.[22]

The location of the implant-abutment interface in relation to the alveolar bone has also been reported to play an important role in bone loss around implants. The presence of an interface at the level of alveolar bone or sub-crestal level is associated with significantly higher inflammatory cell infiltrate and bone loss than when it is at a supra-crestal level.[16]

The design of the implant-abutment interface has an impact on the amount of microbial penetration into the internal parts of dental implants.[52] The structural geometric design of the implant connection (internal or external) is also important to achieve the best implant-abutment interface fit and to favor the stress distribution between connecting components and biological response, hindering microorganism colonization at this interface.[38]

A greater stability of the implant-abutment interface has been correlated to internal connections in which the abutments walls are in close contact with the internal surface of the implant, reducing the possibility of micro-movements during loading.[4, 24] However, studies have shown no significant difference in microgap values as influenced by implant connection.[8, 24]

The material property of the abutment plays an important role in the microgap at the implant-abutment interface. Commercially premachined abutments are available in titanium, zirconia, and zirconia with titanium connections. In order to provide more versatility in overcoming angulation and esthetic problems, castable abutments using plastic burn-out patterns that can be cast with various alloys were introduced.[24, 54]

Titanium abutments were used traditionally as they displayed superior mechanical properties and excellent biocompatibility. They prevent the occurrence of galvanic and corrosive reactions at the implant-abutment interface, enhancing the peri-implant soft tissue health.[27] However, restorations in anterior esthetic zone may warrant the use of ceramics for both abutment and crown as it would provide more translucency as opposed to metal abutments and ceramometal crowns. Alumina was the first ceramic abutment material introduced followed by zirconia that offered better mechanical and optical properties.[8] Zirconia is now available both as premachined as well as custom- machined (CAD-CAM) abutments. Ceramic abutments would be preferable to metal components because of the gray color

that can be transmitted through the peri-impant tissues with metal components.[8] Additionally, these abutments are also non-toxic, have good tissue compatibility and intrasulcular adaptability.[59] Bacterial adhesion to zirconia has also been reported to be low when compared to titanium.[40] Zirconia abutments are preferred over alumina abutments because of their superior fracture resistance, and radio-opacity.[58]

The microgap of the titanium abutment to titanium implant interface has been widely documented in terms of precision of fit.[12, 13, 28] Premachined titanium abutments have shown lesser microgap when compared to castable abutments with various alloys. This is attributed to the possible irregularities in casting procedures.[9, 10, 17, 24, 53, 57] The implant-abutment interface of zirconia abutments with titanium connections has also been studied and found to be similar to machined titanium abutments.[19] However, there are limited studies on the fit at implant-abutment interface using premachined complete zirconia abutments.[5, 8, 59]

During function, clinical loading may result in micromotion in stable implant screw joint, which contributes to screw loosening and increase in microgap at the implant-abutment interface.[12] This is followed by plaque retention at the interface, resulting in clinical sequelae such as bone loss, peri-implantitis and possible loss of osseointegration.[7, 36, 59] A cyclic loading test is intended to simulate components in function, which permits analysis of possible interaction between microgap and loading.[24] While there are many

studies that report this increase in microgap for titanium abutment-to-titanium implant interface,[20, 24, 31, 59] the effect of cyclic loading on zirconia abutment-to-titanium implant interface is inadequately documented. [59]

The various measuring analytical techniques employed for gap measurement at the implant-abutment interface as suggested by previous researchers include scanning electron microscopy (SEM),[5, 19, 23, 59] scanning laser microscopy (SLM),[55] optical microscopy,[10,24] reflex microscopy, travelling microscope, liquid strain gauges,[31] gas permeability,[54] radiography,[46, 49] laser videography, and photoprogrammetric techniques.[22] Video measuring system (VMS 2010-F) has been used in engineering and biomedical fields for measuring microgap with accuracy of upto 1 μm.

In view of the above, the aim of the present in vitro study was to comparatively evaluate the microgap of premachined titanium and zirconia abutments at the implant-abutment interface, before and after cyclic loading

The objectives of the present study included the following:

1. To measure the microgap at the implant-abutment interface between premachined titanium abutments and titanium implants before cyclic loading.
2. To measure the microgap at the implant-abutment interface between premachined titanium abutments and titanium implants after cyclic loading.

3. To measure the microgap at the implant-abutment interface between premachined zirconia abutments and titanium implants before cyclic loading.
4. To measure the microgap at the implant-abutment interface between premachined zirconia abutments and titanium implants after cyclic loading.
5. To compare the microgap at the implant-abutment interface between premachined titanium abutments and titanium implants before and after cyclic loading.
6. To compare the microgap at the implant-abutment interface between premachined zirconia abutments and titanium implants before and after cyclic loading.
7. To compare the microgap at the implant-abutment interface between premachined titanium and zirconia abutments before cyclic loading.
8. To compare the microgap at the implant-abutment interface between premachined titanium and zirconia abutments after cyclic loading.

REVIEW OF LITERATURE

Binon PP (1996)[11] evaluated the effect of misfit between the implant external hexagonal extension and the abutment internal hexagonal recess on abutment screw loosening during simulated function. This study indicated that there was a direct correlation between hexagonal misfit and screw joint loosening. Greater the hexagonal misfit, greater the probability of screw loosening. A rotational misfit of under 2 degree provided the most stable and predictable screw joint.

Binon PP et al (1996)[12] used the rebroaching technique to evaluate the elimination of rotational misfit on screw joint stability. External hexagon implants of known dimensions were assembled with premachined, cast and rebroached cast abutments. The abutment screws were tightened to 20 Ncm and 30 Ncm, and the same were loaded off axis with 133.3 N. They concluded that there was a direct correlation between rotational misfit and screw loosening. Screw joints can be made more resistive to screw loosening by the elimination of rotational misfit.

Dellow AG et al (1997)[22] conducted a study using scanning electron microscope (SEM) to investigate the implant abutment interface fit of four implant systems, as well as the implant-abutment fit when interchanged among the four systems. They concluded that no significant differences in microgap values found when interchanging components. Microgap

measurements were small between implant and abutment when interchanging components, indicating good machining tolerances.

Gratton DG et al (2001)[27] investigated dental implant screw joint micromotion and dynamic fatigue as a function of varied preload torque applied to abutment screws when tested under simulated clinical loading. They observed that the 16 Ncm group exhibited greater micromotion ($P<0.001$) than both the 32 and 48 Ncm groups at all cycle intervals (2-way ANOVA, Tukey HSD). Micromotion of the implant-abutment interface remained constant ($P=.99$) for each of the preload groups through 105 cycles. Under the loading parameters of this study, no measurable fatigue of the implant-abutment interface occurred. However, dental implant screw joints tightened to lower preload values exhibited significantly greater micromotion at the implant-abutment interface.

Hoyer SA et al (2001)[30] investigated the fatigue life of UCLA-style abutment screws in wide-diameter versus conventionally sized dental implant restorations. They found that the dental implant-abutment interface of 3.75mm and 6.0mm externally hexed implants experienced similar joint opening after periods of dynamic loading. Laboratory adjustment of the interface significantly decreased the service life of the abutment screw joint.

Lang LA et al (2003)[36] assessed the precision of fit of CAD/CAM (Procera) abutment internal hexagon and 5 external hexagon implant systems.

They concluded that the Procera custom abutment internal hexagon fit the external hexagon of all implant systmens used tin the study, the Procera abutment screw fit the internal screw bore of the implant systems and that Procera abutment could be considered for universal application with the implant systems studied.

Broggini N et al (2006)[15] compared the distribution and density of inflammatory cells surrounding implants with a subcrestal, crestal, or supracrestal implant-abutment interface. They found that all implants developed a similar pattern of peri-implant inflammation: a nuetrophilic polymorphonuclear leukocytes maximally accumulated at or immediately coronal to the interface. However, peri-implant neutrophil accrual increased progressively as implant-abutment interface depth increased, i.e., subcrestal interfaces promoted a significantly greater maximum density of neutrophils than did supracrestal interfaces. Moreover, inflammatory cell accumulation below the original bone crest was significantly correlated with bone loss. They concluded that implant-abutment interface dictates the intensity and location of peri-implant inflammatory cell accumulation, a potential contributing component in the extent of implant-associated alveolar bone loss.

Vigolo P et al (2006)[57] assessed the rotational freedom between the hexagonal extension of the implant and hexagonal counterpart of the abutment for Procera abutments made with different type of materials (titanium, zirconia and alumina). The results of the study suggested that all types of CAD/CAM

Procera abutments consistently showed less than 3 degrees of rotational freedom between the implant and abutment in case of hexagonal external connection.

Canullo L et al (2007)[18] analyzed the behavior of a biocomponent abutment made of a titanium post luted to a custom-made zirconia abutment using anaerobic cement. They concluded that the abutment's metallic core was necessary to recreate the internal connection with acceptable precision and completely "metal free" abutments are only possible for external hexagon systems. The breakage involved separation of the components without observed fractures.

Coelho AL et al (2007)[21] developed a technique to evaluate the implant-abutment gap of an external hexagon implant system as a function of radius. Implant-abutment gap distances were recorded along the implant-abutment region for each section. Individual measurements were related to their radial position through trigonometric inferences. All implants presented communication between external and internal regions through connection gaps and inaccurate implant-abutment alignment. Polynomial lines showed implant-abutment gap values below 10 μm from 0 μm to approximately 250 μm of the implant-abutment engagement region. Gap distances significantly increased from approximately 250 μm to the outer radius of the implant-abutment engagement region.

Jaime AP et al (2007)[31] evaluated the effect of cast rectifiers on the misfit of cast UCLA abutments compared to premachined UCLA abutments. The influence of casting and porcelain baking on the marginal misfit of these components was also investigated. They concluded that the use of rectifiers in cast UCLA abutments reduced significantly the marginal misfit at the implant-abutment interface. Even with carefully performed laboratory steps, changes at implant interface of premachined UCLA abutments occurred. Porcelain baking did not alter the marginal misfit values of UCLA abutments.

Kano SC et al (2007)[33] conducted a study to propose a classification system based on the horizontal and vertical microgap of the implant-abutment interface. They classified microgap as (1) ideal relationship, (2) horizontal discrepancy only, (3) vertical discrepancy only and (4) both horizontal and vertical discrepancy. Premachined cast-on abutments had significantly higher horizontal misfit than cast NiCr abutments ($P < .001$). In the proposed classification system, 23% of all sites measured at the implant-abutment interface had an ideal relationship, 34% had a horizontal discrepancy only, 4% had a vertical discrepancy only, and 39% had both vertical and horizontal discrepancies. They concluded that the proposed implant-abutment classification system demonstrated a way to characterize and compare the microgap at the implant-abutment interface.

Barbosa GAS et al (2008)[8] investigated whether there is a direct correlation between the level of vertical misfit at the abutment/implant

interface and torque losses in abutment screws. They concluded that there was no significant correlation between the values of vertical misfit at the implant/abutment interface and the values of torque losses applied over the UCLA abutment screws. These findings indicate that great vertical misfits do not necessarily imply higher detorque values.

Steinebrunner L et al (2008)[49] evaluated the influence of long-term dynamic loading on the fracture strength of different implant-abutment connections. Six implant systems were tested: two systems with external connections and four systems with internal connections. Fracture strength was tested with and without dynamic loading. Dynamic loading was performed in a two-axis chewing simulator with 1,200,000 load cycles at 120 N. They concluded that implant systems with long internal tube-in-tube connections and cam-slot fixation showed advantages with regard to longevity and fracture strength compared with systems with shorter internal or external connection designs.

Tiossi R et al (2008)[52] analyzed the fit of 3- unit implant-supported frameworks cast in Nickel- Chromium and Cobalt-Chromium alloys and commercially pure titanium after casting, laser welding and simulated porcelain firing. This study found that Ni-Cr alloy presented the lowest misfit values. After the welding procedures, lower misfit values on the opposite side showed better passivity, though complete passivity could not be assumed since the misfit values were still lower on the tightened side.

Yüzügüllü B et al (2008)[58] assessed the changes in implant-abutment interface of titanium, alumina and zirconia abutments placed on Branemark implants subjected to a standard dynamic loading regimen and evaluated by scanning electron microscopy analysis. They found that after dynamic loading, there was no significant difference between aluminum oxide, zirconium oxide, and titanium abutment groups regarding the microgap at the implant-abutment interface.

Nascimento C et al (2009)[40] investigated the influence of repeated tightening of the abutment screw on leakage of Streptococcus mutans along the interface between implants and pre-machined abutments. They found microorganisms were found on the internal surfaces of both groups evaluated. However, bacterial counts in group 2 were significantly higher than that in the control group ($P<0.05$). These results suggest that bacterial leakage between implants and abutments occurs even under unloaded conditions and at a higher intensity when the abutment screw is tightened and loosened repeatedly.

Tesmer M et al (2009)[51] aimed to use an in vitro model to assess the potential risk for invasion of oral microorganisms into the FAI microgap of dental implants with different characteristics of the connection between the fixture and abutment. Thirty implants were divided into three groups ($n = 10$ per group) based on their microgap dynamics. Groups 1 and 2 were comprised of fixtures with internal Morse-taper connections that connected to standard abutments and the same abutments with a 0.5-mm groove modification,

respectively. Group 3 was comprised of implants with a tri-channel internal connection. They concluded that differences in implant designs may affect the potential risk for invasion of oral microorganisms into the FAI microgap.

Tsuge T et al (2009)[55] evaluated the effect of eccentric cyclic loading on abutment screw loosening in internal and external hexagon implants with either of these two screw materials, titanium (Ti) alloy versus gold alloy. The reverse torque value of the abutment screw was measured before (initial preload) and after loading (post-loading). In all the groups, post-loading preload was significantly higher than initial preload. They concluded that the implant-abutment connection did not have an effect on screw loosening, but the abutment screw material did. In particular, Ti abutment screws were less likely to come loose.

Alves da Cunha TM et al (2010)[4] compared the vertical gap of zirconia Procera® abutment associated with implants from the same manufacturer (Procera manufacturer) and two other implant systems. They concluded that the association of Procera zirconia abutment with other implant systems different from its manufacturer demonstrated significant alteration of vertical misfit at implant-abutment interface.

Baixe S et al (2010)[7] evaluated the microgap between zirconia and titanium abutments, and precision of fit between internal and external implant connections. The results of the study demonstrated smaller microgaps between

implants and zirconia abutments compared to those described in the literature for titanium abutments. The mean microgap was larger for flat-to-flat interface systems, compared to conical interface systems. The authors suggested that precise fit of these abutments could lead to less biologic and biomechanical risk.

Pappavassiliou H et al (2010)[43] investigate the accuracy of conservative dental radiography to detect marginal gaps at the implant-abutment interface. For these reasons radiographs were taken on internal and external hex implants with different experimental gaps and inclinations. They found that there were significant differences between the internal and external hex implants because of the different morphology of the implants. The detecting ability to diagnose a gap at the implant-abutment interface varied significantly with the angulation degree of the X-ray tube. To achieve accurate results, the use of a paralleling device is advocated in order to achieve greater detection ability.

Rack A et al (2010)[45] investigated the micro-gap formation at the implant–abutment interface of two-piece dental implants using high-resolution radiography in combination with hard X-ray synchrotron radiation. Images were taken with the specimen under different mechanical loads of up to 100 N. They found that synchrotron-based radiography in comparison with classical laboratory radiography yields high spatial resolution in combination with high contrast even when exploiting micro-sized features in highly attenuating

objects. The first illustration of a micro-gap which was previously indistinguishable by laboratory methods underlines that the complex micro-mechanical behavior of implants requires further in vitro investigations where synchrotron-based micro-imaging is one of the prerequisites.

Ricomini Filho AP et al (2010)[47] evaluated the preload loss and bacterial penetration through the implant-abutment interface of conical and external hexagon connection systems subjected to thermal cycling and mechanical fatigue (TM). Four different implant-abutment connection systems were evaluated (n=6): external hexagon with universal post, Morse taper with universal post, Morse taper with universal post through bolt, and locking taper with standard abutment. The bacterial penetration was assessed and the abutments were observed by scanning electron microscopy. They found that all screw abutment systems showed significantly higher ($p<0.05$) detorque values when subjected to TM and all conical systems presented bacterial penetration. The results show no relationship between the preload loss and the bacterial penetration.

Asvanund P et al (2011)[6] compared the load transfer characteristics of a complete-arch restoration supported by 4 implants with external and internal implant-abutment connections. Loads were applied to the prostheses in 3 positions. Two-dimensional photoelastic models were used to simulate bone. Two types of implants were placed in the photoelastic models. Complete-arch metal frameworks were fabricated on the abutments. Artificial teeth were

arranged on the framework, and the prosthesis was screwed onto the abutments. The specimens were analyzed at 2 levels (implant-abutment level and apical to the implant level) with 3 loading conditions (4-point load; 2-point anterior load; and 2-point lateral load). They concluded that when loaded off-center, the internal-implant abutment connection produced less stress when compared with the external-implant abutment connection. Therefore, The internal-implant abutment connection could potentially reduce stresses within the connection when off-center loads are applied.

de Torres EM et al (2011)[24] compare stresses transmitted to implants from frameworks cast using different materials and to investigate a possible correlation between vertical misfits and these stresses. The stresses transmitted to implants were measured using quantitative photoelastic analysis in values of maximum shear stress (τ), when each framework was tightened to the photoelastic model to a 10 N cm standardized torque. They observed that correlations between vertical misfits and stresses around the implants were not significant as for any evaluated materials.

De Jesus Tavarez RR et al (2011)[23] evaluated the vertical misfit at the implant/abutment interface of premachined cast-on and premachined abutments of external and internal connections before and after cyclic loading. They concluded that premachined abutments presented better vertical misfit than premachined cast-on abutments for external hex implant connection, for both before and after cyclic loading analysis. Cyclic loading increased the

vertical misfit of premachined cast-on external hex abutments and premachined octagonal internal abutments.

Klotz MW et al (2011)[34] used clinical simulation to determine whether wear of the internal surface of a titanium implant was greater following connection and loading of a one-piece zirconia implant abutment or a titanium implant abutment. They concluded that the implants with the zirconia abutments showed a greater initial rate of wear and more total wear than the implants with the titanium abutments following cyclic loading. The amount of titanium transfer seen on the zirconia abutment increased with the number of loading cycles but appeared to be self-limiting. The clinical ramifications of this finding are unknown at this time; however, the potential for component loosening and subsequent fracture and/or the release of particulate titanium debris may be of concern.

Koutouzis T et al (2011)[35] aimed to use an in vitro dynamic-loading model to assess the potential risk for invasion of oral microorganisms into the fixture-abutment interface microgap of dental implants with different fixture-abutment connection characteristics. Twenty-eight implants were divided into two groups (n = 14 per group) based on their microgap dynamics. Group 1 was comprised of fixtures with internal Morse-taper connection that connected to standard abutments. Group 2 was comprised of implants with a four-groove conical internal connection that connected to multibase abutments. They concluded that differences in implant design may affect the potential risk for

invasion of oral microorganisms into the fixture-abutment interface microgap under dynamic-loading conditions.

Lorenzoni FC et al (2011)[37] evaluated the sealing capability of external hexagon implant systems and assess the marginal fit. Two groups (n = 10 each) were employed: SIN (Sistema de Implantes Nacional, Brazil) and Osseotite, (Biomet 3i, USA). SEM analysis depicted gaps in the implant-abutment interface of both groups. Gaps in the implant-abutment interface were observed along with leakage increased at the 144 hrs evaluation period.

Nayak AG et al (2011)[41] hypothesized that gaps and hollow spaces at the implant abutment interface will act as a bacterial reservoir, which may cause peri implantitis. Hence, they evaluated the sealing ability of O-ring [an addition polysiloxane] and GapSeal [an antibacterial sealing gel]. They concluded that though microbial growth is seen in all the 3 groups, the least growth was seen in Gapseal group followed by o-ring as compared to the unsealed group.

Sharkey S et al (2011)[48] investigated the effect of gap size and the relative angle at which a radiograph was taken on the detection of component misfit. Different types of implant connections (internal or external) and radiographic modalities (film or digital) were assessed. They observed that the relative angulation of the radiograph and the dimension of the gap were the

most significant factors affecting an examiner's diagnostic ability. There were good inter-examiner reliability and neither the type of component used nor the radiographic media used influenced diagnostic ability. They suggested that, angulation of the x-ray beam relative to implant components needs to be controlled when using radiographs to detect component misfit.

Torres JH et al (2011)[53] conducted a study aimed at adapting the gas permeability technique used to assess endodontic sealing to implant-abutment connection leakage. A new nitrogen flow technique was developed for implant-abutment connection leakage measurement, adapted from a recent, sensitive, reproducible and quantitative method used to assess endodontic sealing. The results show very significant differences between various sealing and screwing conditions. The remaining flow was lower after key screwing compared to hand screwing ($p = 0.03$) and remained different from the negative test ($p = 0.0004$). The method reproducibility was very good, with a coefficient of variation of 1.29%. They concluded that the presented new gas flow method appears to be a simple and robust method to compare different implant systems. It allows successive measures without disconnecting the abutment from the implant and should in particular be used to assess the behavior of the connection before and after mechanical stress.

MATERIALS AND METHODS

The present in vitro study was conducted to comparatively evaluate the microgap of premachined titanium and zirconia abutments at the implant-abutment interface before and after cyclic loading.

The following materials and equipments were used for the study:

MATERIALS EMPLOYED:

- Demo titanium dental implant, Standard platform, 3.75mm (Seven, MIS Implants Technologies Ltd., Israel) (Fig.1)
- Implant mount, Standard platform, 3.75mm (MIS Implants Technologies Ltd., Israel) (Fig.2)
- Spirit level indicators (Fig.3)
- Custom-made stainless steel block (Fig.4a & b)
- Clear autopolymerizing acrylic resin (RR Cold Cure, DPI, India) (Fig.5)
- Titanium esthetic abutment, Standard platform, Internal hex, 1mm (MIS Implants Technologies Ltd., Israel) (Fig.6)
- Zirconia abutment, Standard platform, Internal hex, 1mm (MIS Implants Technologies Ltd., Israel) (Fig.7)
- Hex driver, long (MIS Implants Technologies Ltd., Israel) (Fig.8c)
- Hex driver, short (MIS Implants Technologies Ltd., Israel) (Fig.8d)

- Torque wrench with adapter (MIS Implants Technologies Ltd., Israel) (Fig.8 a & b)
- Polyvinyl Siloxane (PVS) impression material – Addition type (Aquasil, Dentsply, Germany)
    - ❖ Soft putty/ Regular set (Fig.9a)
    - ❖ Light body consistency (Fig.9b)
- Auto mixing spiral (Yellow-70 mm, Adenta, USA) (Fid.9c)
- Auto mixing gun (Dispensing Gun 2, Heraeus Kulzer, Dormagen, Switzerland) (Fig.9d)
- Die lubricant (Yeti Dental, Germany) (Fig.10)
- Inlay casting wax (GC Corporation, Tokyo, Japan) (Fig.11)
- PKT instruments (Delta labs, Chennai, India) (Fig.12)
- Sprue wax (Bego, Germany) (Fig.13a)
- Surfactant spray (Aurofilm, Bego, Germany) (Fig.13b)
- Silicone investment ring (Sili Ring, Delta labs, Chennai, India) (Fig.13c)
- Phosphate bonded investment (Bellasun, Bego, Germany) (Fig.13d)
- Colloidal silica (Begosol, Bego, Germany) (Fig.13e)
- Distilled water (Diet Aqua, India)
- Paint brush- small (Kiran series 024 pont, India)
- Ni-Cr alloy pellets (Bellabond plus, Bego, Germany) (Fig.13g)

- Carborundum separating discs (Dentorium, New York, U.S.A.) (Fig.13f)
- Aluminum oxide powder, 100 μm (Delta labs, Chennai, India) (Fig.14)
- Tungsten carbide burs (Edenta, Switzerland) (Fig.15a)
- Silicon carbide rubber points (Dentsply, Germany) (Fig.15b)
- Resin-modified glass ionomer cement (RelyX luting 2, 3M ESPE AG, Seefeld, Germany) (Fig.16)
- Agate plastic spatula (GC Corporation, Tokyo, Japan) (Fig.17a)
- Mixing pad (GC Corporation, Tokyo, Japan) (Fig.17d)
- Plastic instrument (API, Manipal, India) (Fig.17b)
- Hand scaler, anterior (API, Manipal, India) (Fig.17c)
- Custom-made jig (Fig.18)

EQUIPMENTS EMPLOYED:

- Dental surveyor (Saeshin Precision Ind. Co., Korea) (Fig.19)
- Vaccum power mixer (Whipmix, Kentucky, U.S.A.) (Fig.20)
- Burnout furnace (Technico, Technico laboratory products Pvt Ltd., Chennai, India) (Fig.21a)
- Induction casting machine (Fornax, Bego, Germany) (Fig.21b)
- Sandblaster (Delta labs, Chennai, India) (Fig.22)
- Alloy grinder (Demco, California, U.S.A.) (Fig.23)

- Video Measuring System VMS-2010F (CIP Corporation, Korea) (Fig.24)
- Custom-made cyclic loading machine (Fig.25 & 26)

Description of the custom-made cyclic loading machine:

In the present study, a cyclic loading machine was custom-fabricated to simulate components in function, which permitted analysis of possible interaction between the microgap and loading. It consisted of a motor with gearbox, which when rotated, compressed a spring. The spring applied a load, which was transmitted to the test sample. The individual components and the calibration are described below:

Specification of motor:

90 watts, Single phase 230V, Continuous rating, motor giving 1350 RPM with gear reduction box of 1:18 giving a final RPM of 75 (Swipfe Industries, Pune, India).

Specification of spring:

Spring load spring ISO 10243:2010 (Special Springs, Rosa, Italy)

Hole diameter – 16 mm, Rod diameter – 8 mm

Free Length of spring – 38 mm

Spring constant – 48.5 N/mm

Specification of timer:

999 minutes timer with time memory (K-Pas, Chennai, India)

The motor was connected to an eccentric cam of 2.5 mm, which rotated when the motor was turned on. The 2.5 mm eccentric cam compressed a spring to the same length as it rotated generating a load of approximately 120 N. The spring transmitted the load to the stylus (3 mm diameter), which transmitted a lesser load of approximately 109 N to the sample due to energy loss.

Calibration of custom-made cyclic loading device:

The maximum and minimum loads delivered by the custom-made cyclic loading device were calibrated by a professional load calibration agency (Hi Tech Calibration Services, Chennai, India).

Calibrated Results:

Mode: Auto

Max. Load: 109.49 N, Min. Load: -6.52 N

Mode: Manual

Max. Load: 117.83 N, Min. Load: -7.97 N

Description of Video Measuring System:

Video measuring system consists of a movable platform on which the samples are placed, a camera (Sony ½ inch color CCD) capable of 0.7 – 4.5X zoom magnification giving a total magnification of 30 – 190 X, and a computer equipped with a software (M2D-IMG measuring software) for taking measurements with 1 μm sensitivity. It also provides surface and transmission illumination. The samples are placed on the platform under the camera. The light source attached to the camera as well as the source in the platform illuminates the samples so that they can be seen clearly. The magnification can be adjusted to the desired level and focused for a clear magnified image of the samples. By adjusting the knobs on the platform, the samples can be moved in four directions to view different areas of the samples. The magnified images of the samples are projected on the computer screen, which is facilitated by the software. Using the software, both linear and angular measurements are possible and the magnified images on the screen can also be captured and saved for later reference.

Description of Custom- made Jig:

The custom-made jig consists of a platform and bolt. The sample when placed in the jig platform is positioned at 30° angulation and can be secured in place with the help of a bolt.

METHODOLOGY:

I. Preparation of stainless steel blocks

II. Placement of implants in the stainless steel blocks

III. Connection of abutments to implants

IV. Fabrication of Ni-Cr cast crowns

   a. Preparation of wax patterns

   b. Spruing the wax patterns

   c. Investing the wax patterns

   d. Burnout procedure

   e. Casting procedure

   f. Divesting and finishing the cast crowns

V. Cementation of Ni-Cr cast crowns

VI. Measurement of the microgap at the implant-abutment interface before cyclic loading

VII. Cyclic loading of the samples

VIII. Measurement of the microgap at the implant-abutment interface after cyclic loading

IX. Statistical analysis

I. Preparation of stainless steel blocks (Fig.4 a & b):

Twenty (20) metal blocks of dimensions 25mm x 25mm x18mm with a cylindrical mold space of diameter 18mm and depth 16mm were

custom-fabricated. Grooves were made in the internal surfaces of the cylindrical mold space to help retain the autopolymerizing acrylic resin.

II. Placement of implants in the stainless steel blocks (Fig.27, 28 & 29):

The custom-made metal blocks were placed on the surveying platform with the mold space facing up and stabilized. The surveying platform of a dental surveyor (Saeshin Precision Ind. Co., Korea) (Fig.19) was made parallel to the floor using spirit level indicators (Fig.27). An unsterile, demo, titanium implant (Seven, Standard platform, MIS Implants Technologies, Israel) (Fig.1) was connected to the implant mount (MIS Implants Technologies, Israel) (Fig.2) with hex driver (MIS Implants Technologies, Israel) (Fig.8c) and positioned in the center of mold space of the custom-made metal block so that the implant was submerged completely in the mold space except for 1 mm at the crest module (Fig.28). Autopolymerizing clear acrylic resin (Cold Cure, DPI, India) (Fig.5) was poured into the mold space and the resin was allowed to polymerize (Fig.29). This procedure was done for all the twenty custom-made blocks. The embedded implants were randomly divided into two groups of ten each (Group I & Group II).

III. Connection of abutments to implants (Fig.30 & 31):

In Group I, ten premachined titanium esthetic abutments (n=10) (Standard platform, Esthetic abutment, internal hex, 1mm, MIS Implants

Technologies, Israel) (Fig.6) were connected to the corresponding implants embedded in the stainless steel block with the hex driver (MIS Implants Technologies, Israel) and torqued to 30 Ncm using a torque wrench (MIS Implants Technologies, Israel) (Fig.8a), as recommended by the manufacturer (Fig.31). The samples were then labeled as T1 to T10.

In Group II, ten premachined zirconia abutments (n=10) (Standard platform, zircon 1 mm, internal hex, MIS Implants Technologies, Israel) (Fig.7) were connected to the corresponding implants embedded in the stainless steel block with the hex driver (MIS Implants Technologies, Israel) (Fig.8c) and torqued to 30 Ncm using a torque wrench (MIS Implants Technologies, Israel) (Fig.8a), as recommended by the manufacturer (Fig.32). The samples were labeled as Z1 to Z10.

IV. Fabrication of Ni-Cr cast crowns:

a) Preparation of wax patterns (Fig.32)

The screw access hole of the abutment was filled and sealed off with polyvinyl siloxane (Aquasil soft putty, Denstply, Germany) (Fig.9). The abutment was coated with die lubricant (Yeti Dental, Germany) (Fig.10) and excess lubricant was removed using a gentle stream of compressed air. Wax-up of central incisor was done with inlay casting wax (GC Corporation, Tokyo, Japan) (Fig.11). The cingulum of the central incisor was contoured to create a flat surface at a 30 degree inclination to the long

axis of the tooth (Fig.32). An index (Fig.33a) was made of this wax-up using light body and soft putty consistencies of polyvinyl siloxane impression material (Aquasil, Denstply, Germany) (Fig.9) and used to fabricate the pattern for all test samples. Thus, 20 wax patterns were prepared.

b) Spruing the wax patterns (Fig.34a)

The wax pattern was sprued with preformed wax sprue (Bego, Germany) (Fig.13a) of 2.5 mm diameter. The wax sprue was attached to the incisal edge of the pattern and a reservoir was placed 1.5 mm away from the pattern. The pattern was directly sprued to the crucible former (Fig.13c) of the ringless casting system (Sili Ring, Delta labs, Chennai, India) (Fig.34a). All the 20 wax patterns were sprued in an identical manner.

c) Investing the wax patterns (Fig.34b)

All the 20 wax patterns were invested individually using graphite free, phosphate-bonded investment material (Bellasun, Bego, Germany) (Fig.13d). A 6 mm distance was provided between the patterns and top of the ring. All patterns were sprayed with surfactant spray (Aurofilm, Bego, Germany) (Fig.13b), to aid in better wetting of the investment material. As per the manufacturer's recommendation, 160 gm of the phosphate-bonded investment was mixed with 38 ml of investment liquid, which was prepared by missing 30 ml of colloidal silica (Begosol, Bego, Germany) (Fig.13e) and 8 ml of distilled water in the ratio of 3:1. The investment powder was first hand mixed with a spatula until the entire material was

wetted thoroughly followed by vacuum mixing for 30 seconds using vacuum power mixer (Whipmix, Kentucky, U.S.A.) (Fig.20). Once the investment was mixed the entire pattern was painted with a thin layer of investment using a small paintbrush. The sili ring was positioned on the crucible former and the remainder of investment was vibrated slowly in to the ring (Fig.34b). The invested patterns were allowed to bench set for 20 minutes, and the sili ring was removed.

d) Burn out procedure

All the invested patterns were placed in a burnout furnace (Technico, Technico laboratory products Pvt. Ltd., Chennai, India) (Fig.21a) for pattern elimination. Investments with the patterns were left in the burnout furnace for a period of three hours. During the first hour, the temperature was raised from room temperature to 380^{o}C; in the second hour, the temperature was raised to 900^{o}C and during the last hour the temperature was sustained at 900^{o}C to accomplish complete burnout of the pattern without any residue. The investment mold was initially placed in the furnace such that the crucible end was in contact with the floor of the furnace for the escape of molten material. The investment mold was reversed later near the end of burnout cycle with the sprue hole facing upward to enable escape of the entrapped gases and also to allow oxygen contact to ensure complete burnout of the wax pattern.

e) Casting procedure

Casting was accomplished with Ni-Cr alloy (Bellabond plus, Bego, Germany) (Fig.13g) melted in an induction casting machine (Fornax, Bego, Germany) (Fig.21b). The casting procedure was performed quickly to prevent heat loss resulting in thermal contraction of the mold. The Ni-Cr alloy was heated sufficiently till the alloy ingot turned to molten state and the crucible was released. The centrifugal force ensures the complete flow of the molten metal into the mold space.

f) Divesting and finishing the cast crowns (Fig.35a, b & c)

Following casting, the hot casting was allowed to cool to room temperature. A knife was used to trim the investment at the bottom end of the ring. It was then broken apart and the remaining investment was slowly removed (Fig.35a). Adherent investment was removed from the casting by air abrading with 110 μm alumina (Delta labs, Chennai, India) at 80 psi pressure in a sand blasting machine (Delta labs, Chennai, India) (Fig.35b). Sprue was cut using 0.7 mm thin separating discs (Dentorium, New York, U.S.A.) (Fig.13f). The casting was inspected under magnification for casting defects. Casting with irregularities in the internal margin, distorted surfaces were discarded. External surfaces were relieved of all nodules with a round carbide bur (Fig.15a). This procedure was performed for all twenty cast crowns. All the cast crowns were finished using metal trimming burs (Edenta, Switzerland) and silicon carbide rubber points (Fig.15b), white and grey (Dentsply, Germany) (Fig.35c).

V. Cementation of Ni-Cr cast crowns (Fig.36 a & b):

Resin modified glass ionomer cement (RelyX Luting 2, 3M ESPE AG, Seefeld, Germany) (Fig.16), which is available as a two-paste system in clicker was used for cementation of the cast crowns to the abutments. Before cementing the copings, it was ensured that the screw access hole was sealed off with polyvinyl siloxane impression material (Aquasil soft putty, Dentsply, Germany) (Fig.9a). Equal amounts of base and catalyst paste were dispensed on a mixing pad by pressing the clicker. Both the pastes were mixed with folding technique using an agate plastic spatula (GC Corporation, Tokyo, Japan) (Fig.17a) for 30 seconds. The mixed cement was carried to the inner surface of the cast crowns with a plastic instrument (Fig.17b) and painted on the walls (Fig.36a). The cast crowns were then seated on their respective abutments and pressed down with finger pressure for 5 minutes until the initial set (Fig.36b). Excess cement was removed carefully using a hand scaler (API, Manipal, India) (Fig.17c) without scratching the surface of the abutment or implant. The labial, distal, palatal, and mesial surfaces were labeled as 1, 2, 3, and 4 respectively. A total of twenty Ni-Cr cast crowns were cemented to twenty individual samples consisting of ten titanium and ten zirconia abutments connected to their respective embedded implants in the stainless steel blocks. This cemented Ni-Cr cast crowns with the titanium and zirconia abutments were labeled as Group I and Group II test samples respectively (Fig.37a & b).

VI. Measurement of the microgap at the implant-abutment interface before cyclic loading (Fig.38):

The sample with the cemented cast restoration was placed on the platform of video measuring system VMS-2010F (CIP Corporation, Korea) (Fig.38) and the microgap was measured at the implant-abutment interface at 3X zoom lens magnification (Fig.40a & 41a). The measurements were obtained for four surfaces (1, 2, 3 and 4), of each test sample. This was repeated for all twenty samples. Thus, the microgap for ten samples of Group I and ten samples of Group II was measured before cyclic loading and the results were tabulated for statistical analysis.

VII. Cyclic loading of the samples (Fig.39):

Cyclic loading was performed for all 20 samples to simulate oral loading conditions. The sample with the cemented cast restoration was placed in a custom-made jig (Fig.18), which positioned and secured the sample at a 30 degree angle to the floor. This jig was attached to the cyclic loading machine. The stylus was placed on the flattened cingulum portion of the central incisor and it was subjected to cyclic loading (Fig.39). A sinusoidal waveform at 1.25 Hz for load between 0 to 109 N (approximately) simulating human masticatory frequency and loads was applied. This cycle was continued for 630 minutes as set in the timer simulating approximately 47,250 cycles and

45 days of function. Cyclic loading was performed in a dry environment. This procedure was repeated for all twenty samples.

VIII. Measurement of the microgap at the implant-abutment interface after cyclic loading (Fig.38):

After cyclic loading, the sample with the cemented cast restoration was placed on the platform of video measuring system VMS-2010F (CIP Corporation, Korea) and the microgap was measured at the implant-abutment interface at 3X zoom lens magnification (Fig.40b & 41b). The measurements were obtained for four surfaces (1, 2, 3 and 4), of each test sample. This was repeated for all twenty samples. Thus, the microgap for ten samples of Group I and ten samples of Group II was measured after cyclic loading and the results were tabulated for statistical analysis.

IX. Statistical analysis:

The tabulated results were subjected to statistical analysis. All statistical calculations were performed using Microsoft Excel (Microsoft, USA) and SPSS (SPSS for Windows 10.0.5, SPSS Software Corp., Munich, Germany) software. Paired 'T'-Test was used in the comparison of mean microgap values obtained before and after cyclic loading for titanium and before and after cyclic loading for zirconia abutments. Independent 'T'- Test was used to compare the mean microgap values obtained from titanium and zirconia abutments before and after cyclic loading.

METHODOLOGY – OVERVIEW

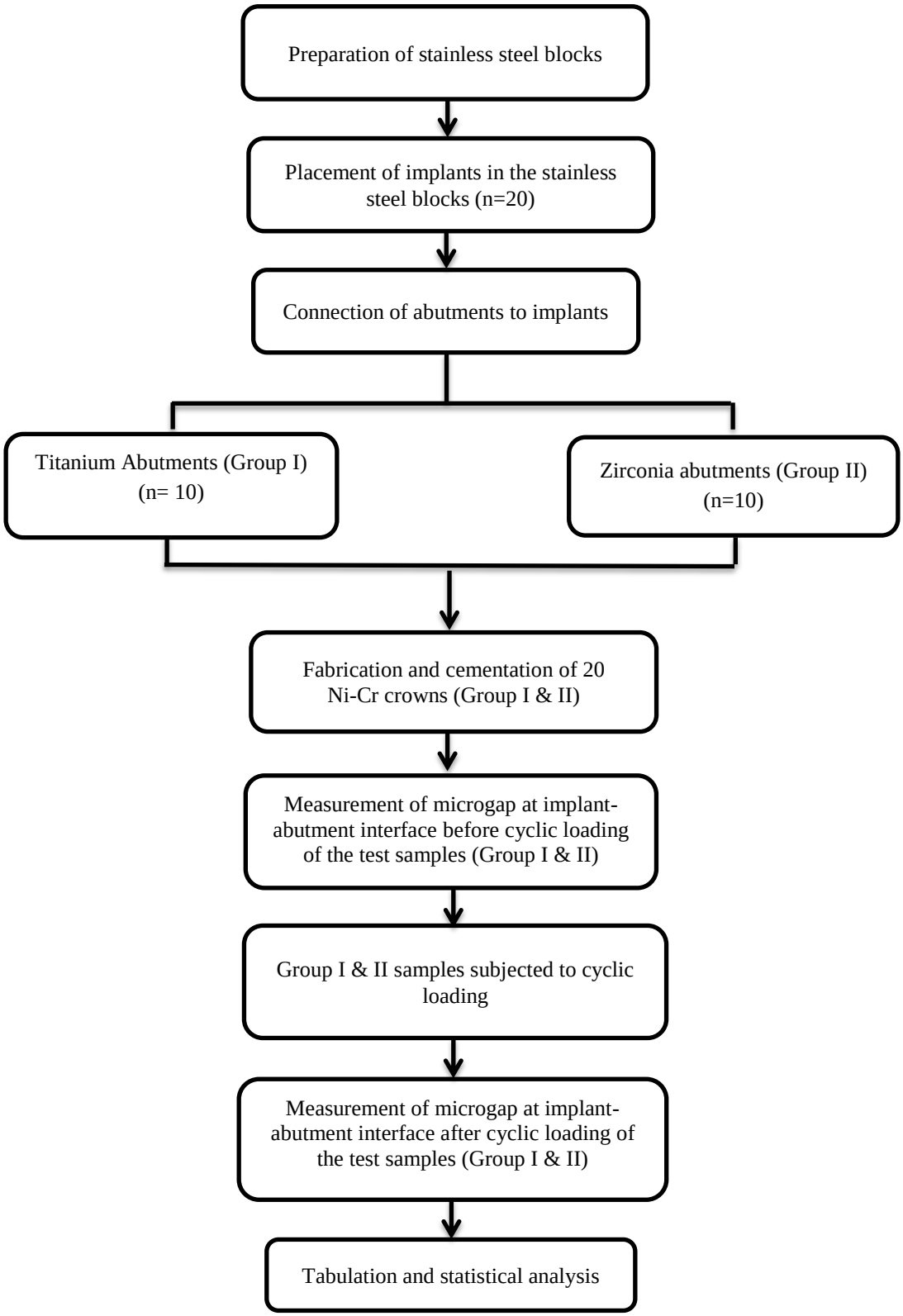

MATERIALS & EQUIPMENTS

Fig.1: Demo titanium dental implant, standard platform, 3.75mm

Fig.2: Implant mount, standard platform, 3.75mm

Fig.3: Spirit level indicators

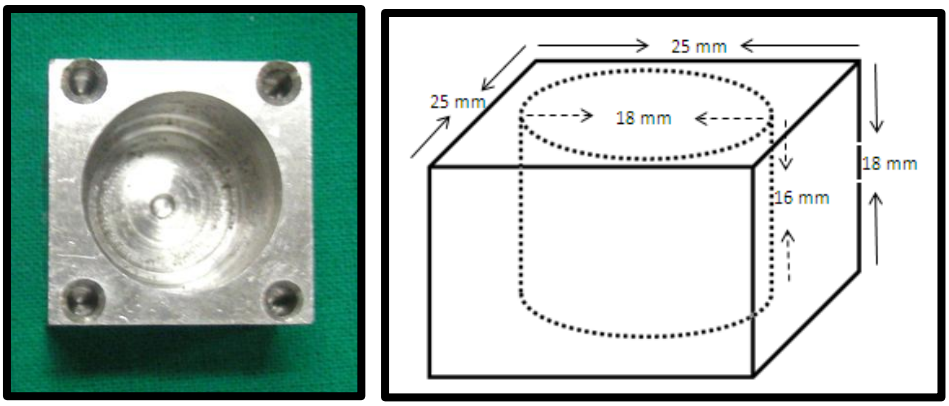

a b

Fig.4a: Custom-made stainless steel block

b: Line diagram of custom-made stainless steel block

Fig.5: Clear auto polymerizing acrylic resin (RR Cold Cure, DPI, India)

Fig.6: Titanium esthetic abutment, standard platform, internal hex, 1mm (MIS Implants Technologies Ltd., Israel)

Fig.7: Zirconia abutment, standard platform, internal hex, 1 mm (MIS Implants Technologies Ltd., Israel)

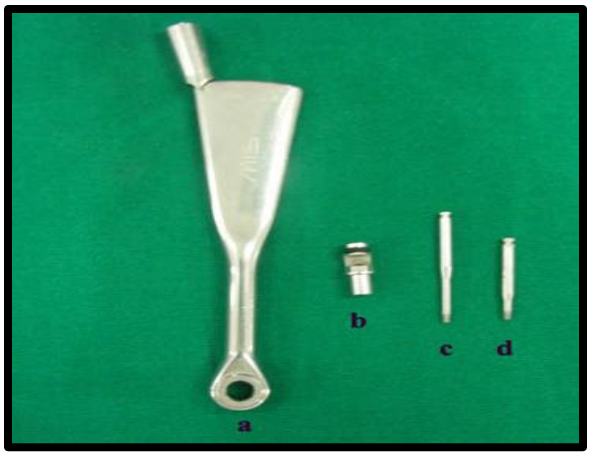

Fig.8a: Prosthetic torque wrench (MIS Implants Technologies Ltd., Israel)

b: Adapter (MIS Implants Technologies Ltd., Israel)

c: Hex driver, long (MIS Implants Technologies Ltd., Israel)

d: Hex driver, short (MIS Implants Technologies Ltd., Israel)

Fig.9a: Soft Putty, Polyvinyl Siloxane (PVS) impression material-Addition type

b: Light Body, Polyvinyl Siloxane (PVS) impression material-Addition type

c: Mixing spiral

d: Automixing gun

Fig.10: Die lubricant

Fig.11: Inlay casting wax

Fig.12: PKT Instruments

Fig.13a: Sprue wax

b: Surfactant spray

c: Investment ring and crucible former

d: Phosphate bonded investment material

e: Colloidal silica

f: Carborundum seperating discs

g: Ni-Cr alloy pellets

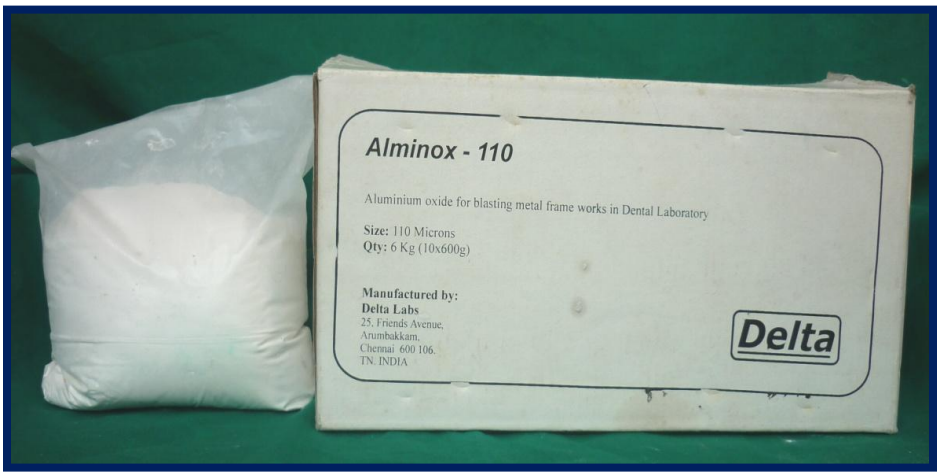

Fig.14: Aluminum oxide powder – 110 µm

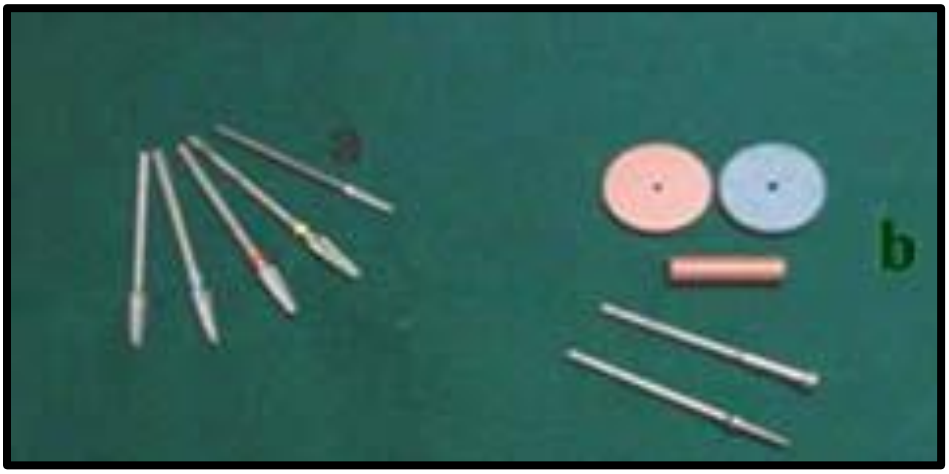

Fig.15a: Tungsten carbide metal trimming burs

b: Silicon carbide rubber points

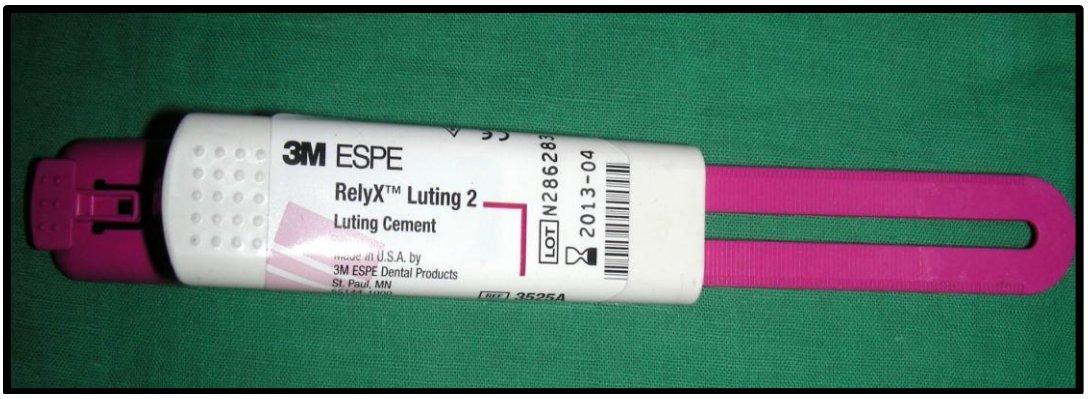

Fig.16: Resin-modified glass ionomer cement

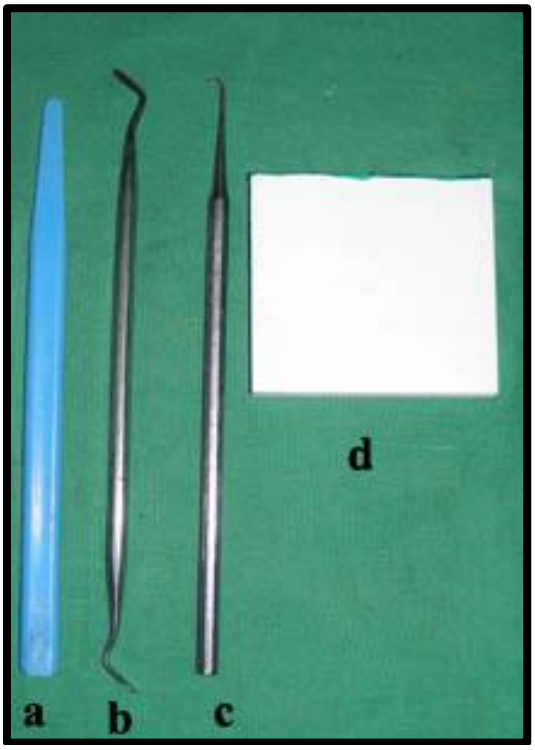

Fig.17a: Agate plastic spatula

b: Plastic instrument

c: Hand scaler

d: Mixing pad

Fig.18: Custom-made jig

Fig.19: Dental surveyor

Fig.20: Vacuum power mixer

Fig.21a: Burnout furnace
b: Induction casting machine

Fig.22: Sandblaster

Fig.23: Alloy grinder

Fig.24: Video Measuring System (VMS)

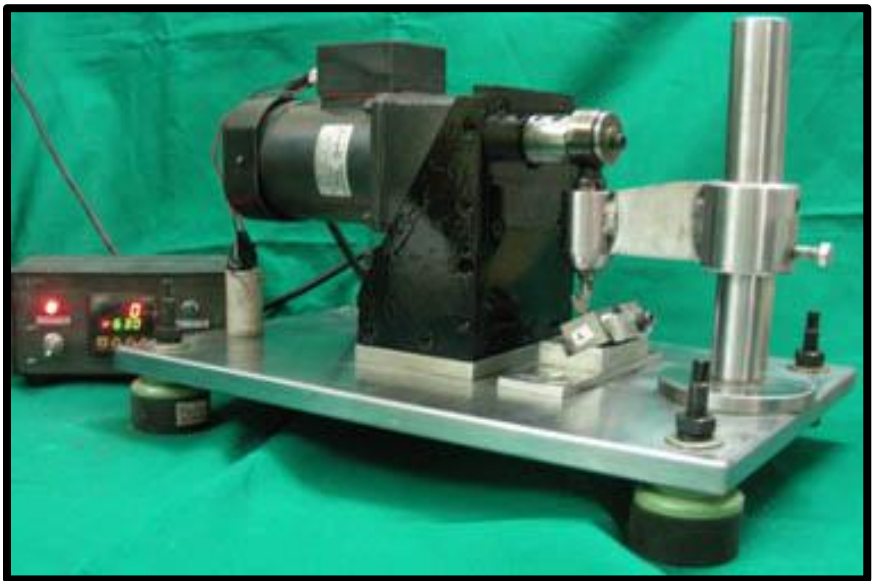

Fig.25: Custom-made cyclic loading machine

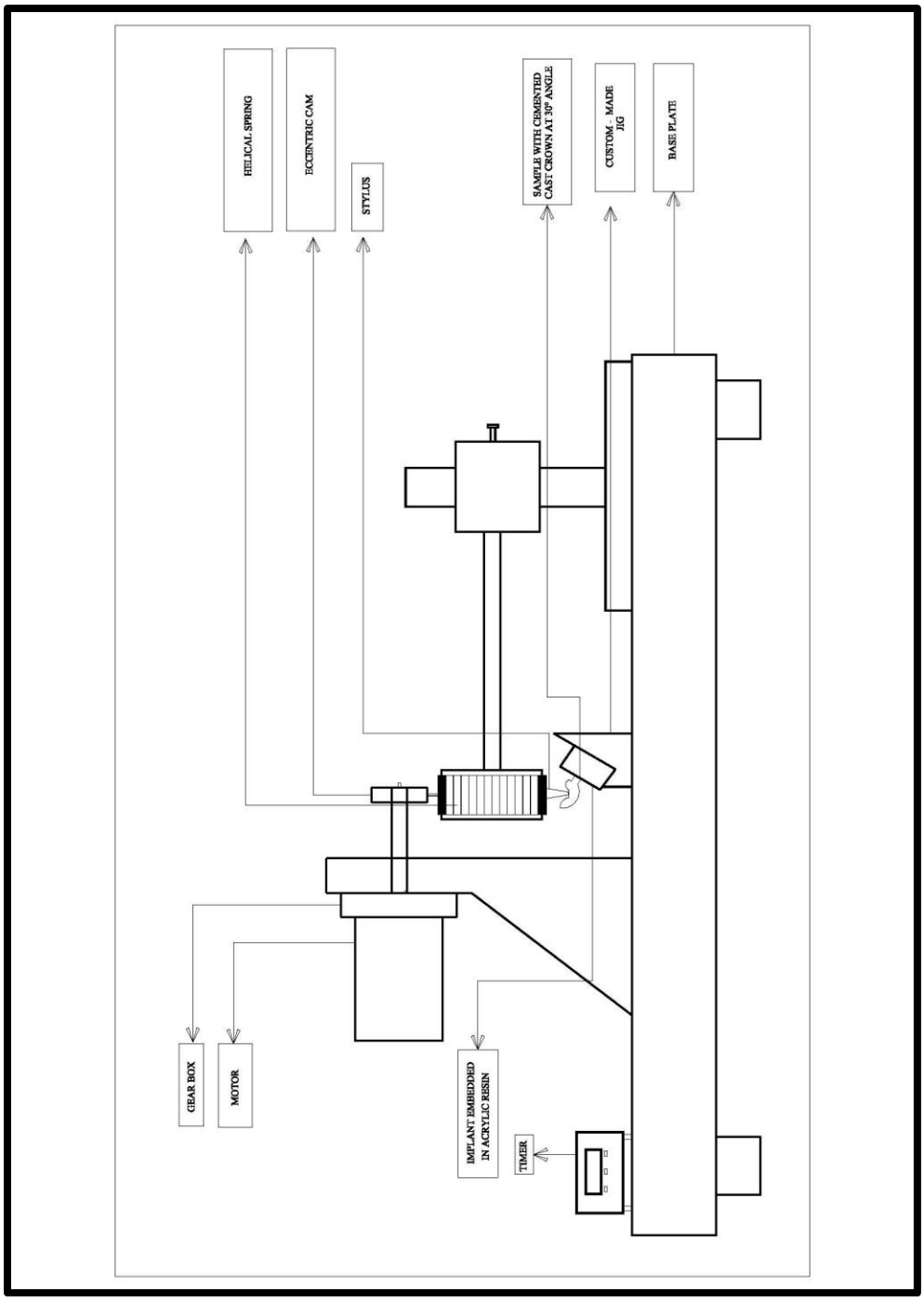

Fig.26: Line diagram for custom-made cyclic loading machine

METHODOLOGY

Placement of implants in stainless steel blocks

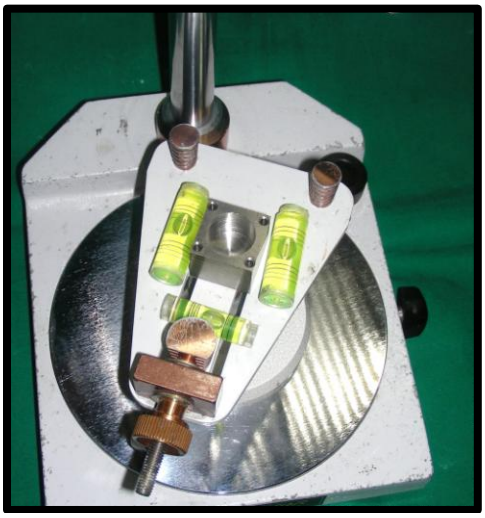

Fig.27: Surveying platform made parallel to floor using spirit level indicators

Fig.28: Positioning of titanium implant in SS block

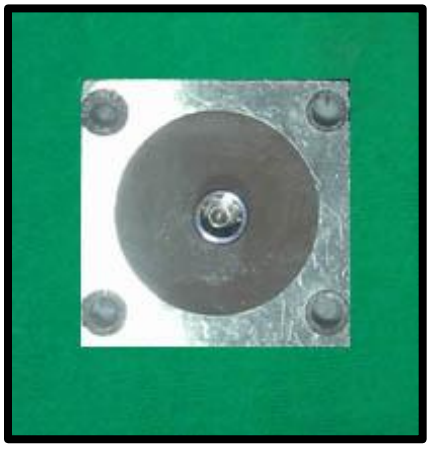

Fig.29: Implant embedded in acrylic resin

Connection of abutments to implants

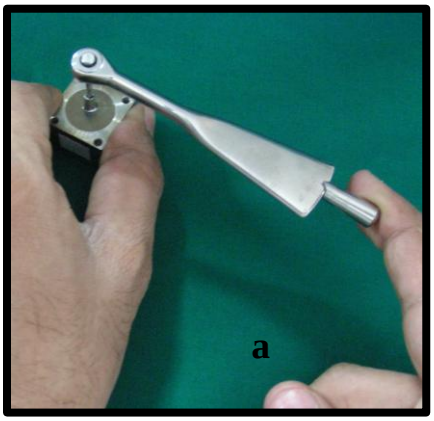

Fig.30a: Torquing of titanium abutment to implant
b: Titanium abutment connected to implant

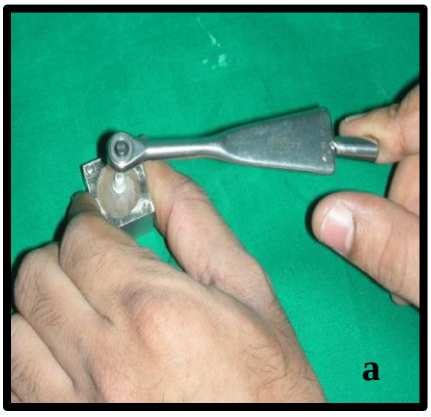

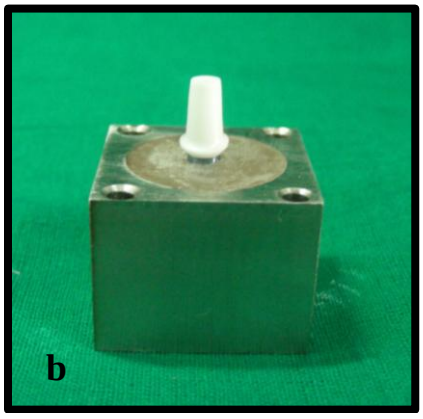

Fig.31a: Torquing of zirconia abutment to implant
b: Zirconia abutment connected to implant

FABRICATION OF Ni-Cr CAST CROWNS

Preparation of wax patterns

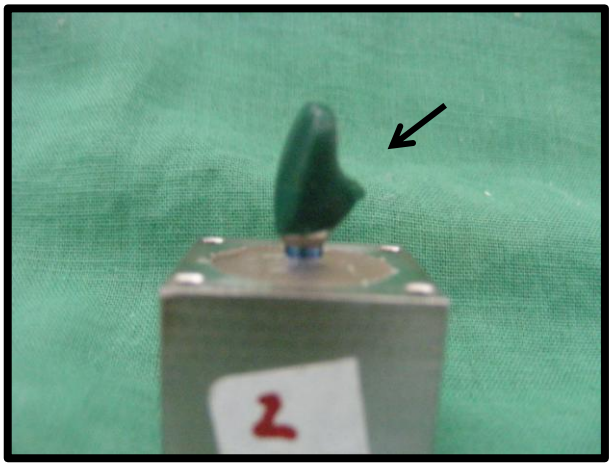

Fig.32: Wax pattern of central incisor with contoured cingulum area

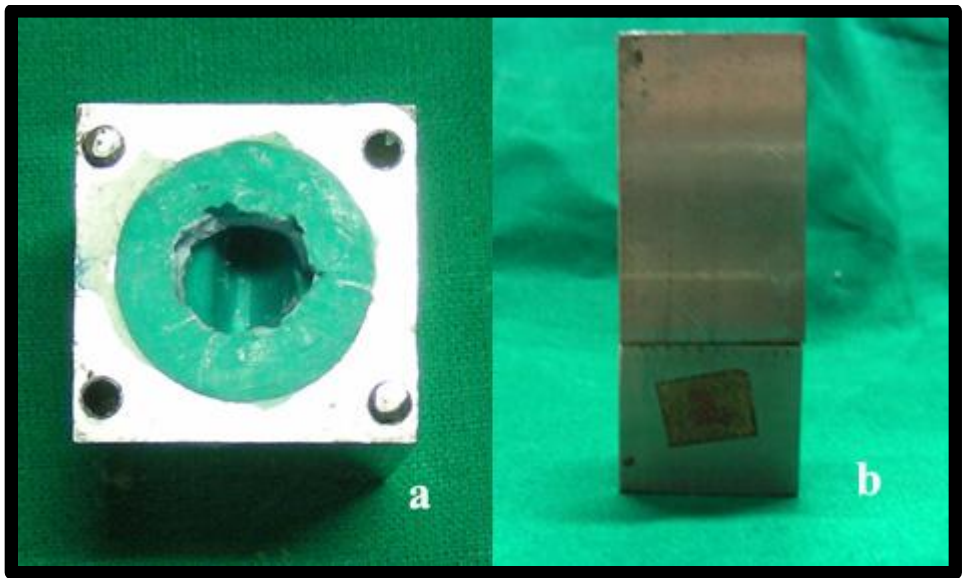

Fig.33a: Index for duplicating the wax patterns
b: Index placed on the custom-made stainless block

Spruing, investing, casting and finishing of Ni-Cr cast crowns

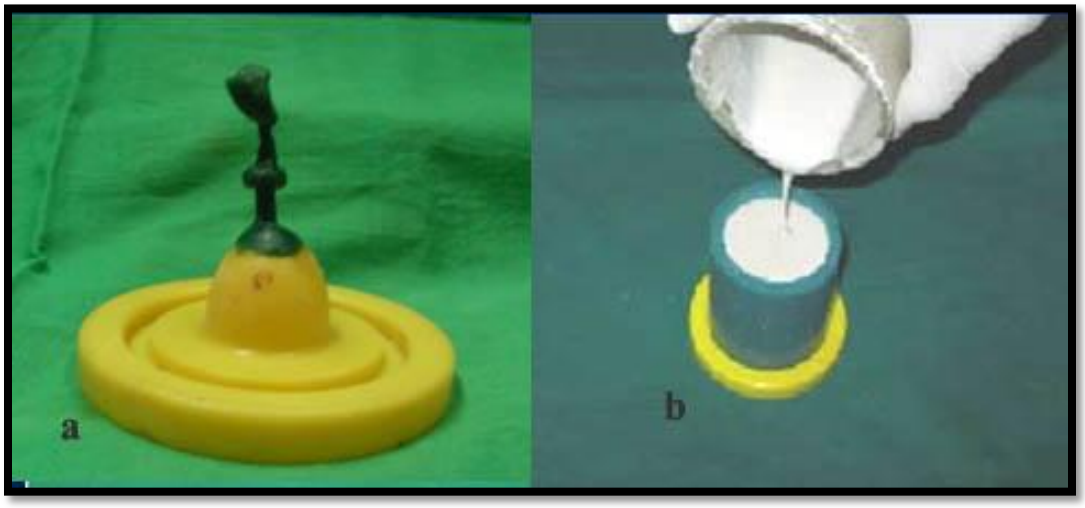

Fig.34a: Pattern attached to crucible former
b: Investing the pattern

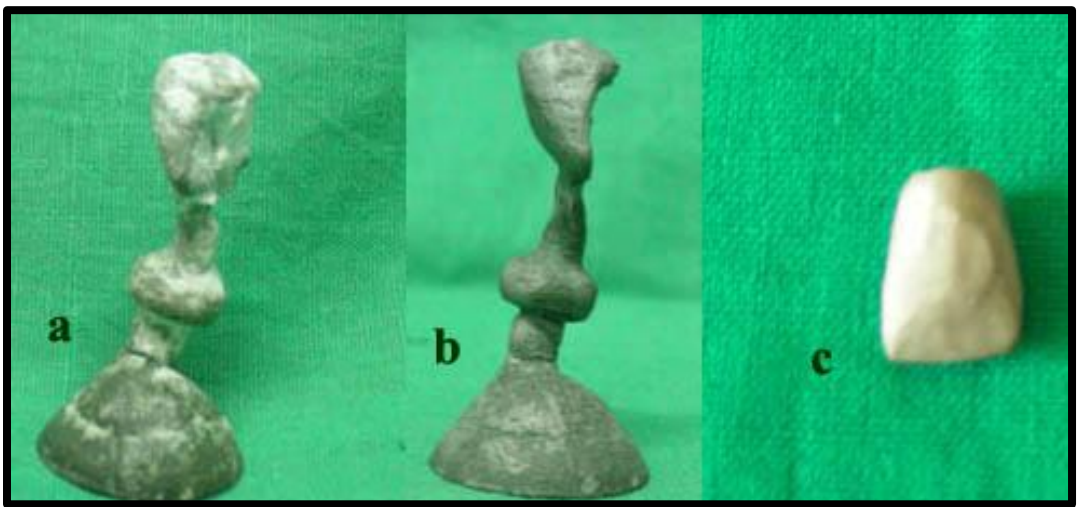

Fig.35a: Divested casting
b: Sandblasted casting
c: Finished crown

CEMENTATION OF Ni-Cr CAST CROWNS

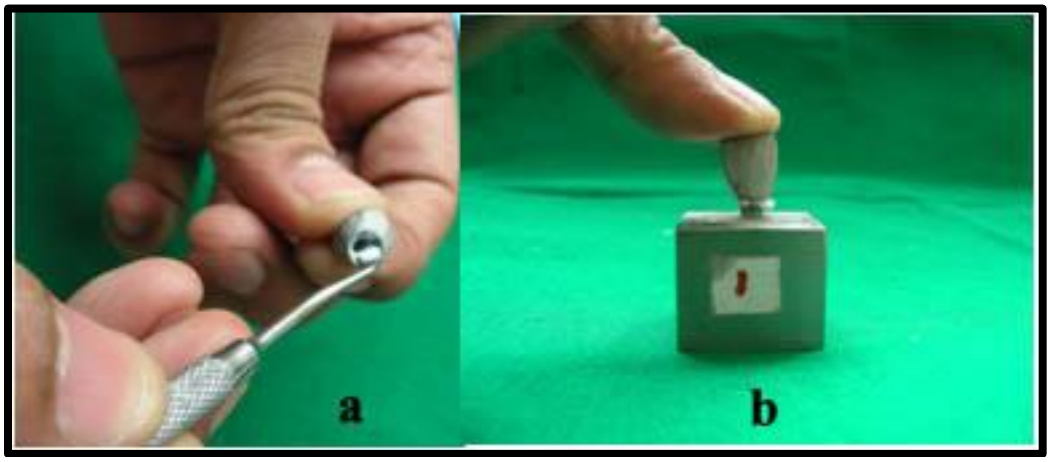

Fig.36a: Mixed cement loaded into the crown
b: Crown seated on the abutment with finger pressure

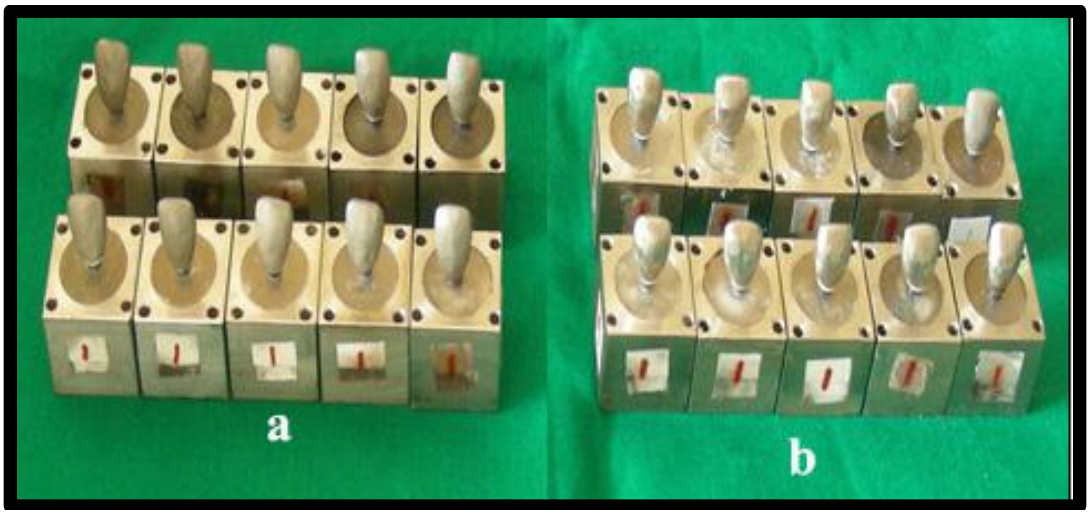

Fig.37a: Group I (Titanium) test samples with cemented crowns
b: Group II (Zirconia) test samples with cemented crowns

Fig.38: Measurement of microgap at implant-abutment interface using Video Measuring System (VMS)

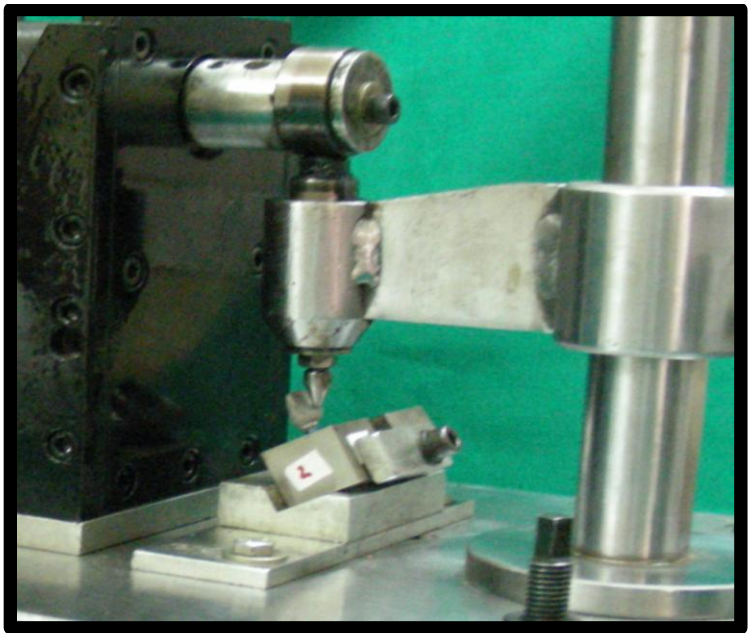

Fig.39: Cyclic loading of test sample

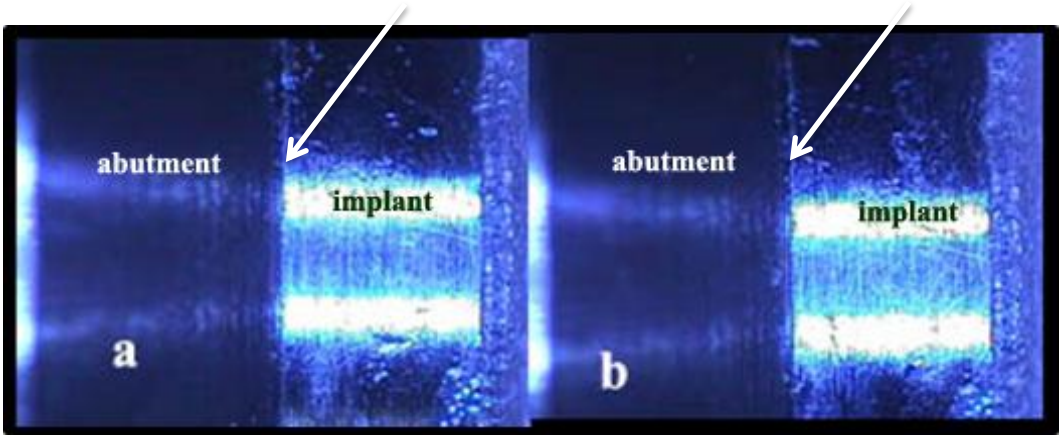

arrows indicate the implant-abutment interface

Fig.40a: VMS image of titanium abutment-implant interface before cyclic loading

b: VMS image of titanium abutment-implant interface after cyclic loading

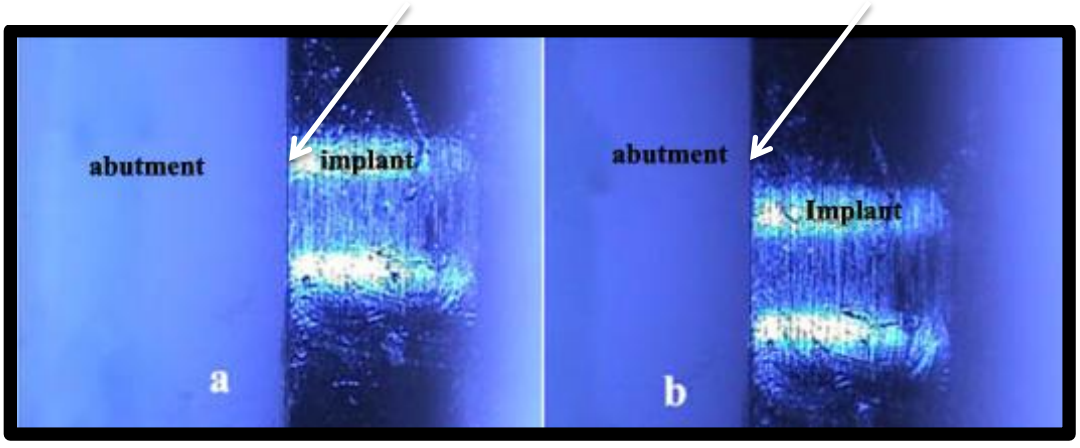

arrows indicate the implant-abutment interface

Fig.41a: VMS image of zirconia abutment-implant interface before cyclic loading

b: VMS image of zirconia abutment-implant interface after cyclic loading

RESULTS

The present in vitro study was conducted to comparatively evaluate the microgap of premachined titanium and zirconia abutments at the implant-abutment interface, before and after cyclic loading.

Twenty titanium implants (Standard platform) were embedded individually into autopolymerizing acrylic resin in custom-made stainless steel blocks. The embedded implants were randomly divided into two groups of ten each (Group I & Group II). In Group I, ten titanium esthetic abutments and in Group II, ten zirconia abutments were connected with a hex driver to their corresponding embedded implants in the stainless steel blocks and torqued to 30 Ncm with a torque wrench. The samples were then labeled as T1 to T10 for titanium abutments and Z1 to Z10 for zirconia abutments. Nickel-Chromium cast crowns were fabricated for all twenty samples and cemented with resin-modified glass ionomer cement. The labial, distal, palatal and mesial surfaces were labeled as 1, 2, 3 and 4 respectively. The microgap was measured at the implant-abutment interface at 3X zoom magnification using video measuring system VMS-2010F for all twenty samples before cyclic loading. The measurements were obtained for four surfaces (1, 2, 3 and 4), of each test sample. The test samples were then subjected to cyclic loading and the microgap was measured again at the implant-abutment interface in the same four surfaces for all 20 samples. The results obtained from the study were tabulated and subjected to statistical analysis.

Table I shows basic values and mean of microgap at the implant-abutment interface of Group I samples (Titanium abutments) before cyclic loading.

Table II shows basic values and mean of microgap at the implant-abutment interface of Group I samples (Titanium abutments) after cyclic loading.

Table III shows basic values and mean of microgap at the implant-abutment interface of Group II samples (Zirconia abutments) before cyclic loading.

Table IV shows basic values and mean of microgap at the implant-abutment interface of Group II samples (Zirconia abutments) after cyclic loading.

Table V shows the comparison between mean values of microgap at implant-abutment interface of Group I samples (Titanium abutments) before and after cyclic loading using Paired 'T'-Test.

Table VI shows the comparison between mean values of microgap at implant-abutment interface of Group II samples (Zirconia abutments) before and after cyclic loading using Paired 'T'-Test.

Table VII shows the comparison between mean values of microgap of Group I (Titanium) and Group II (Zirconia) samples at implant-abutment interface before cyclic loading using Independent 'T'-Test.

Table VIII shows the comparison between mean values of microgap of Group I (Titanium) and Group II (Zirconia) samples at implant-abutment interface after cyclic loading using Independent 'T'-Test.

Table IX shows the comparison between mean values of microgap at implant-abutment interface of Group I (Titanium) and Group II (Zirconia) samples before and after cyclic loading.

Graph I shows basic values of microgap at implant-abutment interface for Group I samples (Titanium abutments) before cyclic loading.

Graph II shows basic values of microgap at implant-abutment interface for Group I samples (Titanium abutments) after cyclic loading.

Graph III shows basic values of microgap at implant-abutment interface for Group II samples (Zirconia abutments) before cyclic loading.

Graph IV shows basic values of microgap at implant-abutment interface for Group II samples (Zirconia abutments) after cyclic loading.

Graph V shows the comparison between mean values of microgap at implant-abutment interface of Group I samples (Titanium abutments) before and after cyclic loading.

Graph VI shows the comparison between mean values of microgap at implant-abutment interface of Group II samples (Zirconia abutments) before and after cyclic loading.

Graph VII shows the comparison between mean values of microgap of Group I (Titanium) and Group II (Zirconia) samples at implant-abutment interface before cyclic loading.

Graph VIII shows the comparison between mean values of microgap of Group I (Titanium) and Group II (Zirconia) samples at implant-abutment interface after cyclic loading.

Graph IX shows the comparison between mean values of microgap at implant-abutment interface of Group I (Titanium) and Group II (Zirconia) samples before and after cyclic loading.

Table I: Basic values and mean of microgap at the implant-abutment interface of Group I samples (Titanium abutments) before cyclic loading

Sample no.	Microgap (µm)				Sample Mean (µm)
	Surface 1	Surface 2	Surface 3	Surface 4	
T1	6	7	9	8	7.50
T2	7	6	7	6	6.50
T3	5	8	9	7	7.25
T4	3	4	8	9	6.00
T5	6	5	7	8	6.50
T6	10	8	8	6	8.00
T7	8	7	8	7	7.50
T8	9	11	4	12	9.00
T9	8	7	5	7	6.75
T10	10	13	6	7	9.00
Group Mean					**7.4000**

Table II: Basic values and mean of microgap at the implant-abutment interface of Group I samples (Titanium abutments) after cyclic loading

Sample no.	Microgap (µm)				Sample Mean (µm)
	Surface 1	Surface 2	Surface 3	Surface 4	
T1	8	9	10	9	9.00
T2	10	7	8	6	7.75
T3	7	10	11	7	8.75
T4	7	5	10	11	8.25
T5	7	8	11	8	8.50
T6	9	8	10	8	8.75
T7	10	9	11	8	9.50
T8	12	13	8	9	10.50
T9	10	9	9	8	9.00
T10	10	12	8	9	9.75
Group Mean					**8.9750**

Table III: Basic values and mean of microgap at the implant-abutment interface of Group II samples (Zirconia abutments) before cyclic loading

Sample no.	Microgap (µm)				Sample Mean (µm)
	Surface 1	Surface 2	Surface 3	Surface 4	
Z1	7	8	8	9	8.00
Z2	9	10	8	9	9.00
Z3	10	8	9	10	9.25
Z4	9	15	9	10	10.75
Z5	7	8	8	9	8.00
Z6	8	10	11	10	9.75
Z7	9	9	8	9	8.75
Z8	11	11	14	12	12.00
Z9	9	9	8	9	8.75
Z10	10	8	10	10	9.50
Group Mean					**9.3750**

Table IV: Basic values and mean of microgap at the implant-abutment interface of Group II samples (Zirconia abutments) after cyclic loading

Sample no.	Microgap (µm)				Sample Mean (µm)
	Surface 1	Surface 2	Surface 3	Surface 4	
Z1	10	9	9	10	9.50
Z2	9	13	10	12	11.00
Z3	8	10	11	11	10.00
Z4	10	12	10	10	10.50
Z5	7	10	10	9	9.00
Z6	9	11	12	9	10.25
Z7	8	8	10	9	8.75
Z8	10	12	9	10	10.25
Z9	8	8	7	10	8.25
Z10	9	8	9	14	10.00
Group Mean					**9.7500**

Table V: Comparison between mean values of microgap at implant-abutment interface of Group I samples (Titanium abutments) before and after cyclic loading using Paired 'T'-Test

GROUP I (T1-T10)	Number of samples	Mean Microgap (μm)	Std.Deviation	P - value
Before cyclic loading	10	7.4000	+/-1.0288	0.000*
After cyclic loading	10	8.9750	+/-0.7857	

P value < 0.05; significant at 5% level

Inference: On statistical analysis using paired 'T'-Test to compare the mean microgap of titanium abutments (Group I) at the implant-abutment interface before and after cyclic loading, it was found that the mean microgap of Group I samples after cyclic loading was higher than the mean microgap before cyclic loading and the P value was <0.05, denoting statistical significance.

Table VI: Comparison between mean values of microgap at implant-abutment interface of Group II samples (Zirconia abutments) before and after cyclic loading using Paired 'T'-Test

GROUP II (Z1-Z10)	Number of samples	Mean Microgap (µm)	Std. Deviation	P - value
Before cyclic loading	10	9.3750	+/-1.2318	0.296
After cyclic loading	10	9.7500	+/-0.8580	

P value < 0.05; significant at 5% level

Inference: On statistical analysis using paired 'T'-Test to compare the mean microgap of zirconia abutments (Group II) at the implant-abutment interface before and after cyclic loading, it was found that the mean microgap of Group II samples after cyclic loading was higher than the mean microgap before cyclic loading and the P value was >0.05, denoting no statistical significance.

Table VII: Comparison between mean values of microgap of Group I (Titanium) and Group II (Zirconia) samples at implant-abutment interface before cyclic loading using Independent 'T'-Test

GROUP	Number of samples	Mean Microgap (µm)	Std. Deviation	P - value
I (T1-T10)	10	7.4000	+/-1.0288	0.001*
II (Z1-Z10)	10	9.3750	+/-1.2318	

P value < 0.05; significant at 5% level

Inference: On statistical analysis using independent 'T'-Test to compare the mean microgap of Group I and II samples at the implant-abutment interface before cyclic loading, it was found that the mean microgap of Group I samples was lesser than the mean microgap of Group II samples and the P value was <0.05, denoting statistically significant difference between the two mean values.

Table VIII: Comparison between mean values of microgap of Group I (Titanium) and Group II (Zirconia) samples at implant-abutment interface after cyclic loading using Independent 'T'-Test

GROUP	Number of samples	Mean Microgap (µm)	Std. Deviation	P - value
I (T1-T10)	10	8.9750	+/-0.7857	0.049*
II (Z1-Z10)	10	9.7500	+/-0.8580	

P value < 0.05; significant at 5% level

Inference: On statistical analysis using independent 'T'-Test to compare the mean microgap of Group I and II samples at the implant-abutment interface after cyclic loading, it was found that the mean microgap of Group I samples was lesser than the mean microgap of Group II samples and the P value was <0.05, denoting statistically significant difference between the two mean values.

Table IX: Comparison between mean values of microgap at implant-abutment interface of Group I (Titanium) and Group II (Zirconia) samples before and after cyclic loading

Loading	Group I (Titanium)	Group II (Zirconia)	P-value
Before cyclic loading	7.40 ± 1.03	9.38 ± 1.23	0.001*
After cyclic loading	8.98 ± 0.79	9.75 ± 0.86	0.049*
P- value	0.000*	0.296	

P value < 0.05; significant at 5% level.

Inference: Statistical analysis with Paired 'T'-test was used to compare the effects of cyclic loading on mean microgap values of Group I and Group II samples. The mean microgap values after cyclic loading were higher than the mean microgap values before cyclic loading for both Group I (Titanium) and Group II (Zirconia) samples. There was a statistically significant increase in the microgap after cyclic loading with Group I (Titanium) samples. The increase in microgap with Group II (Zirconia) samples did not show statistical significance.

Statistical analysis with Independent 'T'-test was used to compare the mean microgap values of Group I and Group II samples before and after cyclic loading. The mean microgap value of Group I (Titanium) samples was lesser than the mean microgap value of Group II (Zirconia) samples, both before and after cyclic loading. There was statistically significant difference between the mean microgap values of Group I (Titanium) and Group II (Zirconia) samples, both before and after cyclic loading.

Graph I: Basic values of microgap at implant-abutment interface for Group I samples (Titanium abutments) before cyclic loading

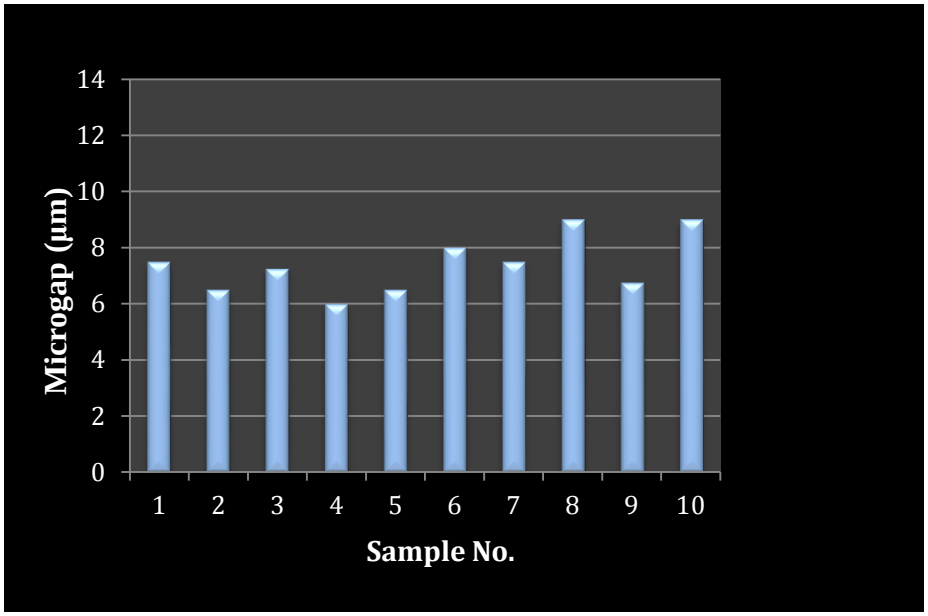

Graph II: Basic values of microgap at implant-abutment interface for Group I samples (Titanium abutments) after cyclic loading

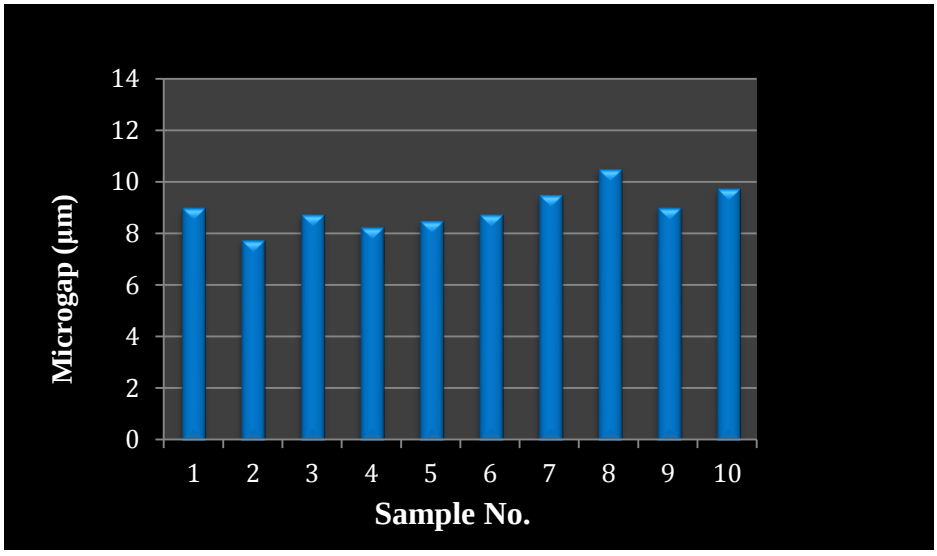

Graph III: Basic values of microgap at implant-abutment interface for Group II samples (Zirconia abutments) before cyclic loading

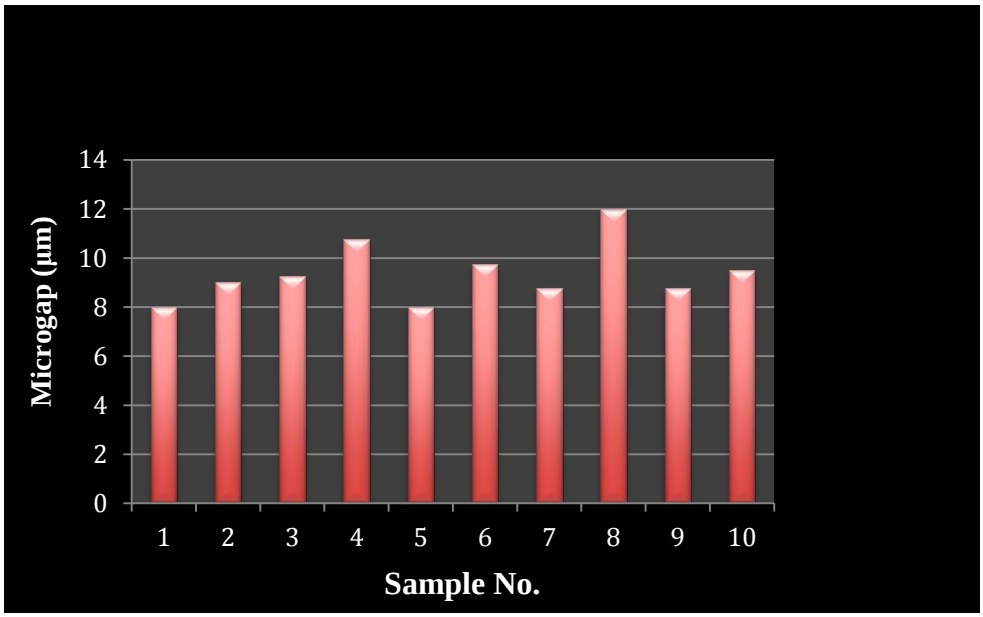

Graph IV: Basic values of microgap at implant-abutment interface for Group II samples (Zirconia abutments) after cyclic loading

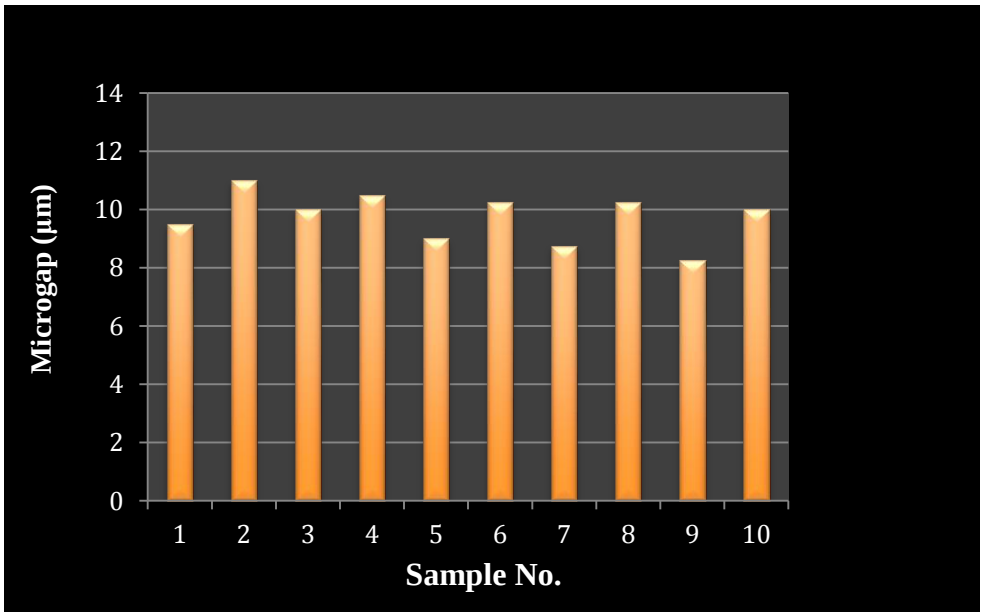

Group V: Comparison between mean values of microgap at the implant-abutment interface of Group I samples (Titanium abutments) before and after cyclic loading

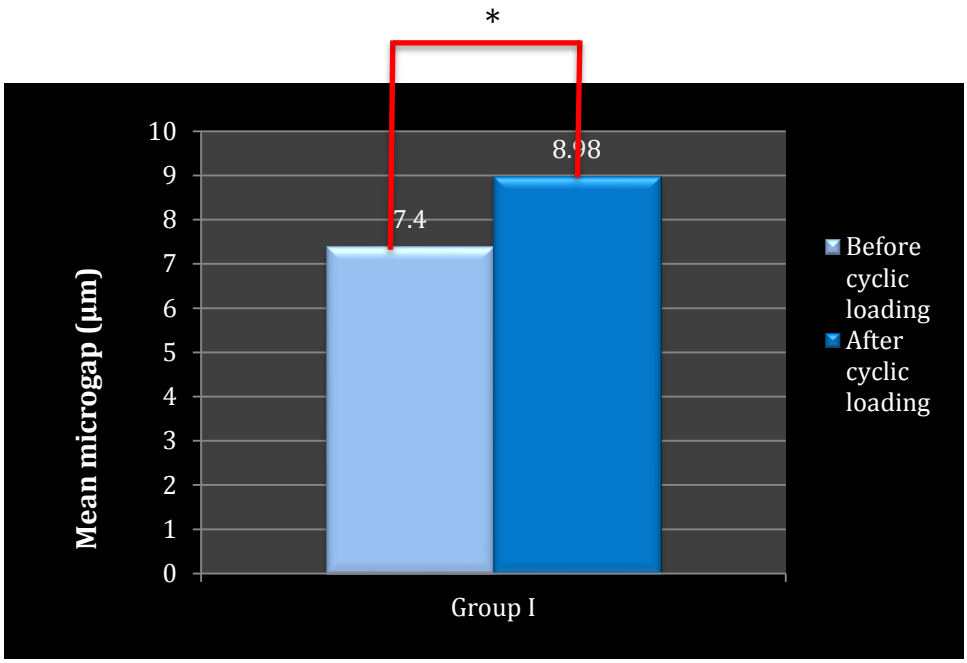

***** Significant at 5% level

Group VI: Comparison between mean values of microgap at the implant-abutment interface of Group II samples (Zirconia abutments) before and after cyclic loading

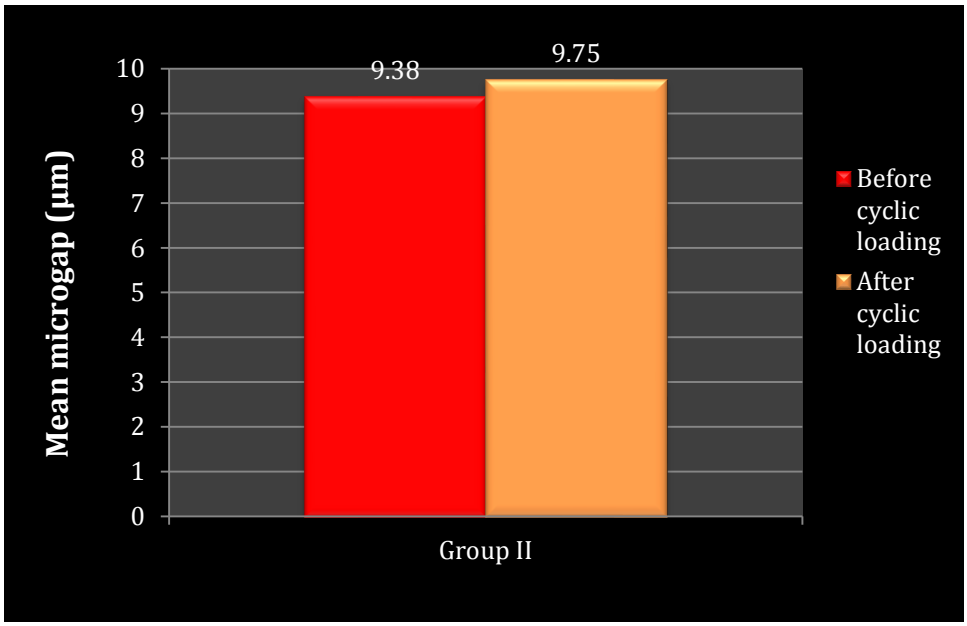

Graph VII: Comparison between mean values of microgap of Group I (Titanium) and Group II (Zirconia) samples at implant-abutment interface before cyclic loading

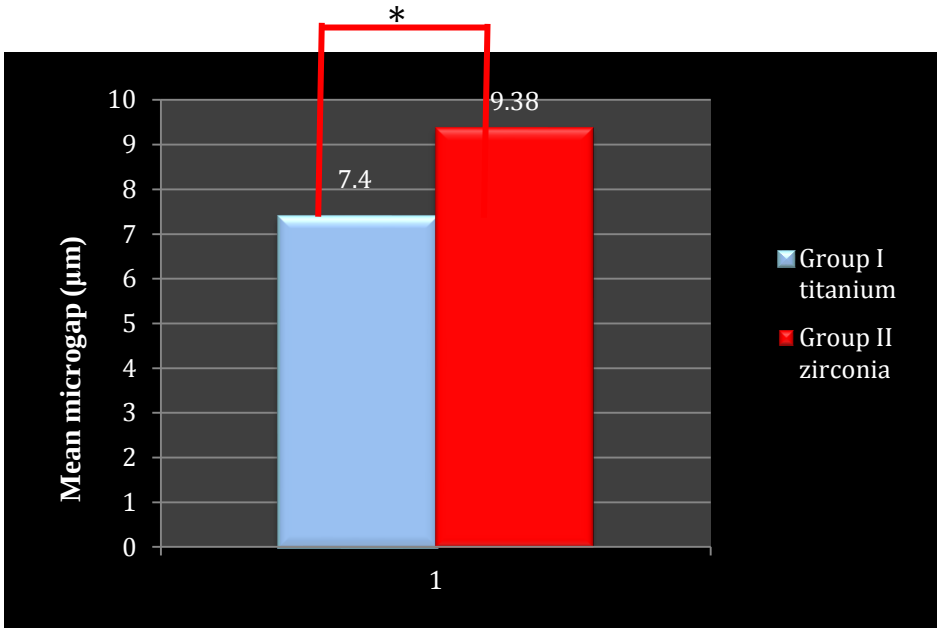

***** Significant at 5% level

Graph VIII: Comparison between mean values of microgap of Group I (Titanium) and Group II (Zirconia) samples at implant-abutment interface after cyclic loading

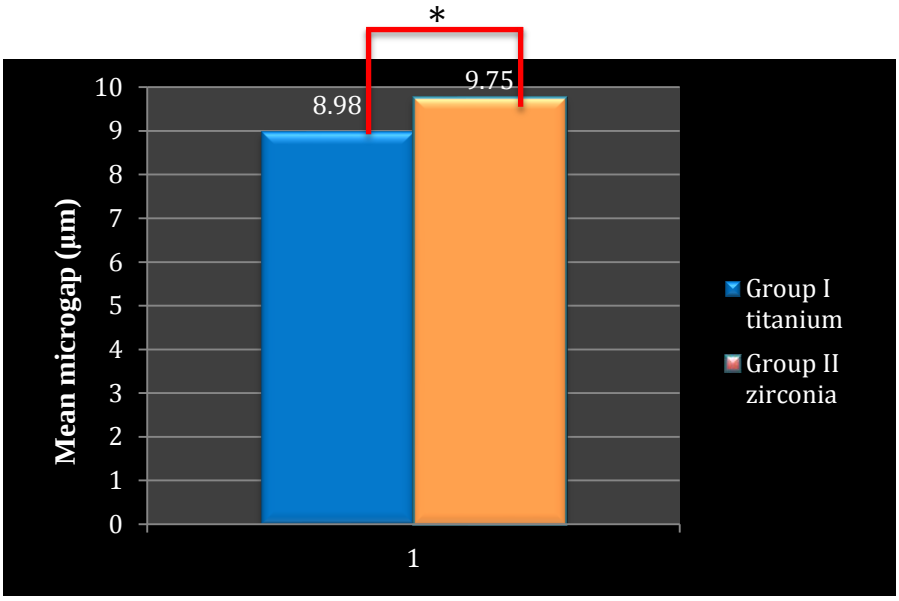

***** Significant at 5% level

Graph IX: Comparison between mean values of microgap at implant-abutment interface of Group I (Titanium) and Group II (Zirconia) samples before and after cyclic loading

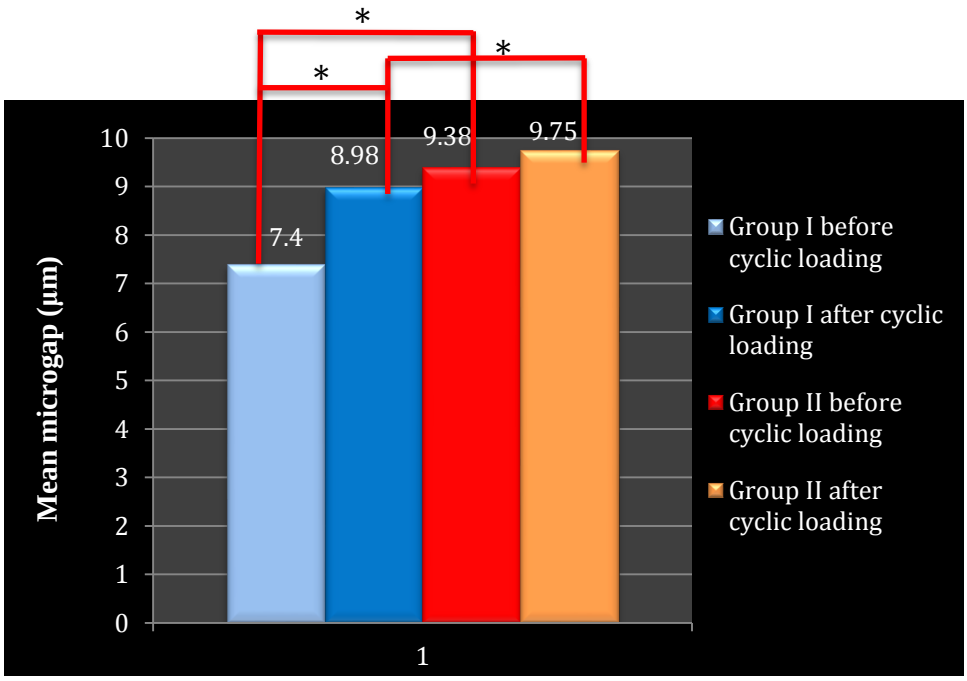

***** Significant at 5% Level

DISCUSSION

The present study was conducted to comparatively evaluate the microgap of premachined titanium and zirconia abutments at the implant-abutment interface before and after cyclic loading.

The precision of fit begins at the junction of the implant and the abutment placed on the implant.[37] When an abutment is connected to the implant fixture, a microgap is created between the components.[52] Although the ideal level of accuracy of fit at the implant-abutment interface is yet to be determined, some authors claim that controlling the amount of misfit is important to prevent mechanical and biologic failures, as well as to maintain osseointegration. [4, 12, 14, 16, 17, 34] In the absence of an ideal level of fit, the recommendation is to choose implant-abutment combinations that have demonstrated acceptable fit in research investigations. Also, various attempts have been made to minimize the microgap at the implant-abutment interface. They include the introduction of wide-diameter implants, the use of platform switching,[18, 21] or the application of dental sealer and O-ring.[42] The microgap of the titanium abutment to titanium implant interface has been widely documented in terms of precision of fit.[12, 13, 28]

The implant-abutment interface of zirconia abutments with titanium connections has also been studied and found to be similar to machined

titanium abutments.[19] However, there are limited studies on the fit at implant-abutment interface using premachined complete zirconia abutments.[5, 8, 59] Also, the effect of cyclic loading on zirconia to titanium interface is inadequately documented. [59] Therefore, the present study was conducted to comparatively evaluate the microgap of premachined titanium and zirconia abutments at the implant-abutment interface before and after cyclic loading.

Unsterile, titanium implants were used in this study as titanium continues to be the most common material used for implant fixtures. Since this was an in vitro study measuring only the effect of mechanical factors on the implant-abutment interface, it was assumed that an unsterile implant would suffice. The type of connection used in the present study was internal hexagon. The internal hexagon configuration has the advantage of reduced vertical height from implant platform to the top of the abutment, distribution of lateral loading deep within the implant leading to a better-shielded abutment screw and long internal wall engagement that creates a stiff, unified body to resist joint micromovement when compared to external hexagon connection implant systems.[7,55] Many studies have been performed using external connection implant systems, while there are limited studies evaluating the misfit using internal hexagon.[24,54] Therefore, internal hexagon implant was used in the present study.

The implants were embedded in autopolymerizing methyl methacrylate resin as it exhibits an elastic modulus similar to that reported for trabecular

bone (1.95 GPa).[59] The entire implant was submerged except for 1 mm at the crest module to allow easy visualization of the implant-abutment interface for taking measurements.

Premachined titanium abutments were used as one of the test materials in the present study as they continue to be the most common abutment material still in use. The microgap of the titanium abutment to titanium implant interface has been widely documented in terms of precision of fit.[12, 13,28] Premachined titanium abutments have shown to have lesser microgap when compared to castable abutments with the use of gold, Ni-Cr alloy, Co-Cr alloy, and cast titanium. This is attributed to the possible irregularities in casting procedures.[9, 10, 17, 24, 53, 57]

Ceramic abutments were introduced to overcome the esthetic drawbacks of titanium abutments as the grey color was transmitted through the peri-implant soft tissue.[8] Zirconia is more commonly used as an esthetic abutment material owing to its superior mechanical and optical properties when compared to alumina.[8] Zirconia is also the only ceramic abutment material that is available as a prefabricated abutment. There are inadequate studies that report the fit of zirconia abutment to titanium implant interface with the use of premachined complete zirconia abutments. Various studies have evaluated the microgap between implant and titanium abutments. Considering the lack of enough studies evaluating the microgap between

premachined zirconia abutments and titanium implants, these abutments were included as one of the test materials in the present study.

Both the premachined titanium and zirconia abutments were connected to their corresponding implants and torqued to 30 Ncm as this was considered as the optimum preload as recommended by the manufacturer for maintenance of screw joint assembly. Preload maximizes the fatigue life, while offering a reasonable degree of protection against screw loosening.[56]

To simulate clinical conditions for transfer of occlusal load to the abutments, Ni-Cr crowns were cast and cemented to the individual samples. The crown resembled a central incisor with the cingulum area contoured to be flat at a 30^{o} angulation to the long axis of the tooth. This facilitated the easy placement and stabilization of the stylus of the custom-made cyclic loading machine. The 30^{o} inclination was given to simulate the occlusal relationship of maxillary and mandibular incisor and to simulate functional stresses along the central incisor root angulation.[59] During transmission of masticatory forces via the restoration-abutment interface to the dental implants, the lateral component of force is thought to be responsible for creating bending moments. On the surface facing the external load, the implant and the abutment experience tensile stresses from bending, while on the opposite surface, the connection is subject to compression. The non-axial forces affecting the anterior maxilla cause higher stresses concentrated along the facial and lingual surfaces of the implant-abutment interface.[59] In the present study, it was for this reason that

cyclic loading was performed at 30^{o} oblique loading, which is more relevant clinically, and could therefore better simulate the mechanical events occurring at the implant-abutment interface. The crowns were cemented with resin-modified glass ionomer cement, as it is one of the commonly used luting agents for cementation purpose.

Many studies have shown the importance of implant-abutment fit, [4, 14, 17] but an agreed-upon standard for measuring microgap has not been established. Many of the techniques established for measuring marginal fit of conventional restorations have been adapted and used for measuring the implant-abutment interface. The various measuring analytical techniques employed for gap measurement include, scanning electron microscopy (SEM),[5,19,23,59] scanning laser microscopy (SLM),[55] optical microscopy[10,24] reflex microscopy, travelling microscope, liquid strain gauges,[31] gas permeability,[54] laser videography, and photoprogrammetric techniques.[22] Some authors have performed radiographs for clinical evaluation of the gap at the implant-abutment interface and concluded that the microgap is influenced by inclination of x-ray tube in relation to the long axis of the implant. [46, 49]

The measuring technique is required to be easy to perform, must provide a repeatable measuring point and have high sensitivity. In the present study video measuring system was used to measure the microgap at the implant-abutment interface in an in vitro setting. Video measuring system consists of a movable platform on which the samples are placed, a camera

(Sony ½ inch color CCD) capable of 0.7 – 4.5X zoom magnification giving a total magnification of 30 – 190 X, and a computer equipped with a software (M2D-IMG measuring software) for taking measurements with 1 μm sensitivity. It also provides surface and transmission illumination. The samples are placed on the platform under the camera. The light source attached to the camera as well as the source in the platform illuminates the samples so that they can be seen clearly. The magnification can be adjusted to the desired level and focused for a clear magnified image of the samples. By adjusting the knobs on the platform, the samples can be moved in four directions to view different areas of the samples. The magnified images of the samples are projected on the computer screen, which is facilitated by the software. Using the software, both linear and angular measurements are possible and the magnified images on the screen can also be captured and saved for later reference. This procedure allowed the use of a repeatable measuring point, so that the samples can be measured both before and after cyclic loading. It was also an easy instrument to use and operate at a low cost.

Clinical loading may result in micromotion in apparently stable implant screw joint and may contribute to screw loosening and prosthesis failure.[12] Cyclic loading of the implant-prosthesis assembly induces micromotion of the joint components, which could wear down the microscopically rough areas of the contacted surfaces, thereby affecting joint stability. The micro-gap between the implant and the abutment may increase

because of bending moments and consecutive fatigue and wear at the interface. This is followed by plaque retention at the interface, resulting in clinical sequelae such as bone loss, peri-implantitis and possible loss of osseointegration.[7, 59] In the present study, a cyclic loading test was performed to simulate components in function, which permitted the analysis of possible interaction between microgap and loading. To accomplish this, a custom-made cyclic loading machine was fabricated with specifications as reported in literature.[33, 56, 59]

A sinusoidal waveform cyclic loading, between 0 to 109 N was applied at a loading rate of 1.25 Hz, which is similar to the reported human masticatory frequency.[33, 56] Cycles were continued for 630 minutes as set in the timer, which simulated approximately 47,250 cycles corresponding to 45 days of function.[59] Breeding et al reported that mechanical failures like screw loosening tend to occur early, usually within the first month of function.[15] Therefore, a 45-day simulation for cyclic loading was used in the present study.

The mean microgap value of premachined titanium abutments at the implant-abutment interface before cyclic loading obtained in the present study was 7.4 μm. Previous researches using machined titanium abutment have shown microgap values ranging from 0 μm to 5.6 μm when implants with internal connection were used.[23, 24, 55] Studies involving machined titanium abutments over external connection implants have reported microgaps at the

implant-abutment interface in the range of 0.32 μm to 7.17 μm.[11, 22, 23, 34, 55,59] The mean value obtained in the present study is less than 10 μm as has been reported in various studies for the vertical microgap between machined components.[11, 33]

The mean microgap value of premachined titanium abutments at the implant-abutment interface after cyclic loading obtained in the present study was 8.9 μm. Mean microgap values ranging from 3 μm to 4.83 μm have been reported in the literature for premachined titanium abutments after cyclic loading.[24, 59] There was a statistically significant ($p < 0.05$) increase in microgap value (1.5 μm) after cyclic loading in the present study. This is consistent with the report of De Jesus Tavarez et al.[24] In contrast Yuzugullu et al[59] has reported a marginal decrease in post cyclic loading microgap value with the use of custom-machined titanium abutments. The possible reason for increase in microgap at the implant-abutment interface is that external forces can create a vibratory movement and cause threads to "back off." The backing off of the threads leads to a reduction in the effective preload and diminishes the ability of the screw to maintain the joint stability thereby increasing the implant-abutment interface gap space.[59] Another explanation is that the thin walls demanded for internal connections could be the weakest point allowing enlargement of the implant upper border during the loading test and increase in vertical microgap.[24] Considering the limited research done on microgap

evaluation after cyclic loading, no definitive conclusions can be drawn with regard to increase in microgap value of premachined titanium abutments.

The mean microgap value of premachined zirconia abutments at the implant-abutment interface before cyclic loading obtained in the present study was 9.4 μm. There is a lack of scientific literature regarding microgap evaluation with the use of premachined complete zirconia abutments for internal hexagon implant systems. Microgap in the range of 0.38 μm to 5.7 μm have been reported with the use of custom-machined zirconia abutments for both internal and external connection implant systems.[5, 8, 59] Canullo et al has reported a mean vertical microgap of 4.4 μm for customized zirconia abutments with titanium connections.[19] The mean value obtained in the current study cannot be directly correlated to those obtained in the previous studies due to the difference in abutment material, type of connection and method of fabrication of abutment.

The mean microgap value of premachined zirconia abutments at the implant-abutment interface after cyclic loading obtained in the present study was 9.7 μm. There was a statistically insignificant ($p > 0.05$) increase in microgap value (0.3 μm) after cyclic loading. Yuzugullu et al[59] had evaluated the effect of dynamic loading on custom-machined zirconia abutments and found a decrease from 2.52 μm to 1.85 μm after dynamic loading. Considering the lack of sufficient literature evaluating the microgap with the use of premachined zirconia abutments, a direct correlation cannot be achieved with

the present study, as there is a difference in type of implant connection used and method employed for fabrication of zirconia abutments. The marginal increase in microgap value (0.3 μm) for premachined zirconia abutments before and after cyclic loading can be attributed to fretting wear occurring after loading in ceramic abutments which may have caused the mating surfaces of ceramic abutments and implants to move closer instead of separating.[59]

The mean microgap values for premachined titanium (7.4μm) and premachined zirconia (9.4μm) abutments at the implant-abutment interface before cyclic loading in the present study were marginally higher than those reported in literature. This can be attributed to the difference in machining tolerance of different implant systems.[5, 23, 59]

On comparison, there was a statistically significant difference in the mean microgap values of premachined titanium and zirconia abutments before cyclic loading. Titanium abutments (7.4μm) exhibited lesser microgap than zirconia abutments (9.4μm) at the implant-abutment interface, but both the values were within the clinically acceptable range (less than 10μm).[25,37,39] This is in contrast to the results achieved by Yuzugullu et al[59] where custom-machined zirconia abutments have shown lesser microgap than custom-machined titanium abutments. This variability could have been due to the physical and mechanical properties of the abutment material used and its influence in machining tolerance of the components.[41] Also, the influence of

sintering of zirconia abutments after machining could affect the fit at the implant-abutment interface.[43]

Comparison of the mean microgap values of premachined titanium (8.9 μm) and zirconia (9.7 μm) abutments after cyclic loading showed statistically significant difference ($p<0.05$) between the values. Both the mean microgap values were within the clinically acceptable range.[25, 37, 39] In general, premachined titanium abutments showed lesser microgap values than zirconia abutments. Also, both the type of abutments used in the present study exhibited an increase in microgap values after cyclic loading.

Considering the values obtained for premachined titanium and zirconia abutments in the present study, it can be concluded that both are suitable implant abutment materials for achieving good fit at the implant-abutment interface. Previous researches with castable abutments using gold, Ni-Cr alloy, Co-Cr alloy and cast titanium have shown microgap values ranging from 7 μm to 29.9 μm before cyclic loading.[10, 24, 34] De Jesus Tavarez et al[24] reported an increase in microgap values of about 5 μm after cyclic loading with cast-on gold abutments. Hoyer et al[31] found an increase in microgap value in the range of 10 μm to 15 μm after 100,000 cycles of loading with the use of gold abutments. The same study reported a reduction in microgap value after 500,000 cycles. These limited studies that evaluated the effect of cyclic loading and varying abutment materials on the microgap at the implant-

abutment interface reveal that the mechanical property of the abutment material influences the fit at the implant-abutment interface.

One of the limitations of the present study was that only a 45-day simulation of cyclic loading was performed. A longer loading period may affect the implant-abutment interface differently. The effect of cyclic loading on mechanical complications like reduction in preload, screw fracture or abutment rotation and on biologic effects like microbial leakage was not evaluated. Further, aging of zirconia has been suggested to cause a progressive transformation of the metastable tetragonal phase into the monoclinic phase, causing degradation of the mechanical properties.[40] In the present study, cyclic loading was performed under dry conditions. Therefore, future studies should verify if the aging process causes critical damage to zirconia abutments.

Future research can include the effect of cyclic loading on microgap of castable abutments using cast titanium, Ni-Cr alloy and Co-Cr alloy at the implant-abutment interface. Also, the influence of duration of cyclic loading and type of implant connection on the microgap can be evaluated. Since there is no scientific support for the clinical belief that misfit alone contributes to clinical problems, in vivo studies regarding bone response to misfit can also be evaluated. More studies assessing the horizontal and rotational misfit as well as stress transfer of zirconia abutments will likely provide better information regarding their clinical use and enhance the results obtained in the present study.

CONCLUSION

The following conclusions were drawn based on the results obtained in this present in vitro study, which was conducted to comparatively evaluate the microgap of premachined titanium and zirconia abutments at the implant-abutment interface, before and after cyclic loading:

1. The mean microgap at the implant-abutment interface between premachined titanium abutments (Group I) and titanium implants before cyclic loading was found to be 7.40 μm.
2. The mean microgap at the implant-abutment (Group I) interface between premachined titanium abutments and titanium implants after cyclic loading was found to be 8.98 μm.
3. The mean microgap at the implant-abutment interface between premachined zirconia abutments (Group II) and titanium implants before cyclic loading was found to be 9.38 μm.
4. The mean microgap at the implant-abutment interface between premachined zirconia abutments (Group II) and titanium implants after cyclic loading was found to be 9.75 μm.
5. On comparison, the mean microgap value at the implant-abutment interface between premachined titanium abutments (Group I) and titanium implants after cyclic loading (8.98 μm) was higher than the mean microgap value before cyclic loading (7.40 μm). This increase in mean value was found to be statistically significant.

6. On comparison, the mean microgap value at the implant-abutment interface between premachined zirconia abutments (Group II) and titanium implants after cyclic loading (9.75 μm) was higher than the mean microgap value before cyclic loading (9.38 μm). This increase in mean value was found to be statistically insignificant.
7. On comparison, the mean microgap value at the implant-abutment interface for premachined titanium abutments (Group I) (7.40 μm) was lesser than that for premachined zirconia abutments (Group II) (9.38 μm) before cyclic loading. The difference in mean values was found to be statistically significant.
8. On comparison, the mean microgap value at the implant-abutment interface for premachined titanium abutments (Group I) (8.98 μm) was lesser than that for premachined zirconia abutments (Group II) (9.75 μm) after cyclic loading. The difference in mean values was found to be statistically significant.
9. On overall comparison, the mean microgap at the implant-abutment interface of premachined titanium abutments was significantly lesser than that of premachined zirconia abutments before and after cyclic loading. Cyclic loading had more effect in increasing the microgap with titanium abutments than with zirconia abutments. The mean microgap values obtained in this study for both Groups were within the clinically acceptable range of 10 μm.

SUMMARY

The present in vitro study was conducted to comparatively evaluate the microgap of premachined titanium and zirconia abutments at the implant-abutment interface, before and after cyclic loading.

Twenty titanium implants (Standard platform) were embedded into autopolymerizing acrylic resin in custom stainless steel blocks and randomly divided into two groups of ten each. In Group I, ten titanium esthetic abutments (Standard platform, 1mm, internal hex) were connected to their corresponding implants and torqued to 30 Ncm. In Group II, ten zirconia abutments (Standard platform, zircon 1 mm, internal hex) were connected to the corresponding implants and torqued to 30 Ncm. Nickel-Chromium cast crowns were fabricated for all twenty samples and cemented with resin-modified glass ionomer cement. The labial, distal, palatal and mesial surfaces were labeled as 1, 2, 3, and 4 respectively.

The test samples were placed on the platform of the video measuring system VMS-2010F and the microgap was measured at the implant-abutment interface. The measurements were obtained for four surfaces (1, 2, 3 and 4), of each test sample. Each sample was sequentially positioned in the jig of a custom-made cyclic loading device at an angulation of 30^{o}, and subjected to cyclic loading for loads between 0 and 109 N at a frequency of 1.25 Hz for 630 minutes. After cyclic loading, the microgap was measured at the implant-abutment interface. The microgap measurement was done individually for all 20 test samples (Group I & II) before and after cyclic loading in a similar

manner. The results obtained from the study were tabulated and statistically analyzed.

The mean microgap at the implant-abutment interface of the premachined titanium samples was higher after cyclic loading than the mean microgap before cyclic loading and this increase in mean values was statistically significant. The mean microgap at the implant-abutment interface of the premachined zirconia samples was also higher after cyclic loading than the mean microgap before cyclic loading. But this increase in mean values was statistically insignificant. Therefore, cyclic loading had more effect in increasing the microgap with premachined titanium abutments than with premachined zirconia abutments.

The mean microgap at the implant-abutment interface for the premachined titanium samples was lesser than the mean microgap for the premachined zirconia samples before and after cyclic loading and they were statistically significant.

These results indicate that cyclic loading had resulted in higher increase in microgap with titanium abutments but, the final microgap value exhibited by those abutments was lesser compared to zirconia abutments.

In this in vitro study, the mean values of microgap obtained was less than 10 μm for both titanium and zirconia samples before and after cyclic loading which is in tune with those obtained in previous studies and considered to be within the clinically acceptable range.[25, 37, 39]

Among premachined abutments, titanium abutments have traditionally been used as the abutment of choice owing to their superior mechanical properties and extensive research done on them. However, restorations in anterior esthetic zone may warrant the use of ceramics for both abutment and crown as it would provide more translucency as opposed to metal abutments and ceramometal crowns. Zirconia abutments would be preferable to titanium abutments because of their esthetic, mechanical and biocompatible properties.

The results in the present study indicates that the premachined zirconia abutments exhibit microgap values within the clinically acceptable range and show their capability in resisting increase in microgap at the implant-abutment interface under cyclic loading. There was an absence of abutment movement, coping, abutment, or screw fracture with zirconia abutments. Therefore, it can be concluded that zirconia abutments can be used for implant-supported restorations in the anterior esthetic zone as an alternative to titanium abutments. Further studies to assess the mechanical properties and long-term clinical studies may be needed to evaluate the performance of zirconia abutments.

BIBLIOGRAPHY

1. **Abrahamsson I, Berglundh T, Glantz PO, Lindhe J.** The mucosal attachment at different abutments. J Clin Periodontol 1998;25:721-727.
2. **Abreu RT, Spazzin AO, Noritomi PY, Consani RLX, Mesquita MF.** Influence of material of overdenture- retaining bar with vertical misfit on three dimensional stress distributions. J Prosthodont 2010;19:425-31.
3. **Albrektsson T.** A multicenter report on osseointergrated oral implants. J Prosthet Dent 1988;60:75-84.
4. **Al-Turki LEE, Chai J, Lautenschlager EP, Hutten MC.** Changes in prosthetic screw stability because of misfit of implant-supported prostheses. Int J Prosthodont 2002;15:38-42.
5. **Alves de Cunha TM, Correia de Araújo RP, Barbosa da Rocha PV, Amoedo RMP.** Comparison of fit accuracy between procera custom abutments and three implant systems. Clin Implant Dent Relat Res 2010 Dec 22. [Epub ahead of print]
6. **Assunção WG, Gomes EA, Rocha EP, Delben JA.** Three-dimensional finite element analysis of vertical and angular misfit in implant-supported fixed prostheses. Int J Oral Maxillofac Implants 2011;26:788-796.

7. **Asvanund P, Morgano SM.** Photoelastic stress analysis of external versus internal implant-abutment connection. J Prosthet Dent 2011;106:266-271.
8. **Baixe S, Fauxpoint G, Arntz Y, Etienne O.** Microgap between zirconia abutments and titanium implants. Int J Oral Maxillofac Implants 2010;25:455-460.
9. **Barbosa GAS, Bernardes SR, das Neves FD, Fernandes Neto AJ, de Mattos Mda G, Ribeiro RF.** Relation between implant/abutment vertical misfit and torque loss of abutment screws. Braz Dent J 2008;19:358-363.
10. **Barbosa GAS, das Neves FD, de Mattos Mda G, Rodrigues RCS, Ribeiro RF.** Implant/abutment vertical misfit of one-piece cast frameworks made with different materials. Braz Dent J 2010;21:515-519.
11. **Binon PP.** Evaluation of machining accuracy and consistency of selected implants, standard abutments, and laboratory analogs. Int J Prosthodont 1995;8:162-178.
12. **Binon PP.** The effect of implant/abutment hexagonal misfit on screw joint stability. Int J Prosthodont 1996;9:149-160.
13. **Binon PP, McHugh MJ.** The effect of eliminating implant/abutment rotational misfit on screw joint stability. Int J Prosthodont 1996;9:511-519.

14. **Binon PP.** Implants and components: Entering the new millennium. Int J Oral Maxillofac Implants 2000;15:76-94.
15. **Breeding LC, Dixon DL, Nelson EW, Tielge JD.** Torque required to loosen single-tooth implant abutment screws before and after simulated function. Int J Prosthodont 1993;6:435-439.
16. **Broggini N, McManus LM, Hermann JS, Medina R, Schenk RK, Buser D, Cochran DL**. Peri-implant inflammation defined by the implant-abutment interface. J Dent Res 2006;85:473-478.
17. **Byrne D, Houston F, Cleary R, Claffey N.** The fit of cast and machined implant abutments. J Prosthet Dent 1998;80:184-92.
18. **Canay S, Akça K.** Biomechanical aspects of bone-level diameter shifting at implant-abutment interface. Implant Dent 2009;18:239-48**.**
19. **Canullo L, Morgia P, Marinotti F.** Preliminary laboratory evaluation of biocomponent customized zirconia abutments. Int J Prosthodont 2007;20:486-488.
20. **Cibirka RM, Nelson SK, Lang BR, Rueggeberg FA.** Examination of implant-abutment interface after fatigue testing. J Prosthet Dent 2001;85:268-75.
21. **Çimen H, Yengin E.** Analyzing the effect of platform switching procedure on stresses in the bone and implant-abutment complex by FEM analysis. J Oral Implantol. 2010 Jul 21. [Epub ahead of print]

22. **Coelho AL, Suzuki M, Dibart S, Da Silva N, Coelho PG.** Cross-sectional analysis of the implant-abutment interface. J Oral Rehabil 2007;34:508-16.
23. **Dellow AG, Driessen CH, Nel HJC.** Scanning electron microscopy evaluation of the interfacial fit of interchanged components of four dental implant systems. Int J Prosthodont 1997;10:216-221.
24. **De Jesus Tavarez RR, Bonachela WC, Xible AA.** Effect of cyclic loading on vertical misfit of prefabricated and cast implant single abutment. J Appl Oral Sci 2011;19:16-21.
25. **de Torres EM, Rodrigues RCS, de Mattos Mda G, Ribeiro RF.** Effect of commercially pure titanium and alternative dental alloys on marginal fit of one-piece cast implant frameworks. J Dent 2007;35:800-5.
26. **Ekfeldt A, Carlsson GE, Börjesson G.** Clinical evaluation of single-tooth restorations supported by osseointegrated implants: A retrospective study. Int J Oral Maxillofac Implants 1994;9:179-183.
27. **Gomes AL, Montero J.** Zirconia implant abutments: A Review. Med Oral Patol Oral Cir Bucal 2011;16:e50-5.
28. **Gratton DG, Aquilino SA, Stanford CM.** Micromotion and dynamic fatigue properties of the dental implant-abutment interface. J Prosthet Dent 2001;85:47-52.

29. **Gross M, Abramovich I, Weiss EI.** Microleakage at the abutment-implant interface of osseointegrated implants: A comparative study. Int J Oral Maxillofac Implants 1999;14:94-100.
30. **Hermann JS, Schoolfield JD, Schenk RK, Buser D, Cochran DL.** Influence of the size of the microgap on crestal bone changes around titanium implants. A histometric evaluation of unloaded non-submerged implants in canine mandible. J Periodontol 2001;72:1372-1383.
31. **Hoyer SA, Stanford CM, Buranadham S, Fridrich T, Wagner J, Gratton D.** Dynamic fatigue properties of the dental implant-abutment interface: Joint opening in wide-diameter versus standard-diameter hex-type implants. J Prosthet Dent 2001;85:599-607.
32. **Jaime AP, de Vasconcellos DK, Mesquita AM, Kimpara ET, Bottino MA.** Effect of cast rectifiers on the marginal fit of UCLA abutments. J Appl Oral Sci 2007;15:169-74.
33. **Jansen VK, Conrads G, Richter EJ.** Microbial leakage and marginal fit of the implant-abutment interface. Int J Oral Maxillofac Implants 1997;12:527-540.
34. **Kano SC, Binon PP, Curtis DA.** A classification system to measure the implant-abutment microgap. Int J Oral Maxillofac Implants 2007;22:879-885.
35. **Klotz MW, Taylor TD, Goldberg AJ.** Wear at the titanium-zirconia implant-abutment interface: a pilot study. In J Oral Maxillofac Implants 2011;26:970-5.

36. **Koutouzis T, Wallet S, Calderon N, Lungren T.** Bacterial colonization of the implant-abutment interface using an in vitro dynamic loading model. J Periodontol. 2011;82:613-8.
37. **Lang LA, Sierraalta M, Hoffensperger M, Wang RF.** Evaluation of the precision of fit between the procera custom abutment and various implant systems. Int J Oral Maxillofac Implants 2003;18:652-658.
38. **Lorenzoni FC, Coelho PG, Bonfante G, Carvalho RM, Silva NRFA, Suzuki M, Silva TL, Bonfante EA.** Sealing capacity and SEM observation of implant-abutment interface. Int J Dent 2011;Jul 2 Epub 2011.
39. **Markarian RA, Ueda C, Sendyk, CL, Lagana DC, Souza RM.** Stress distribution after installation of fixed frameworks with marginal gaps over angled and parallel implants: A photoelastic analysis. J Prosthodont 2007;16:117-122.
40. **Nakamura K, Kanno T, Milleding P, Ortengren U.** Zirconia as dental implant abutment material: a systematic review. Int J Prosthodont 2010;23:299-309.
41. **Nascimento C, Barbosa RES, Issa JPM, Watanabe E, Ito IY, Albuquerque Jr RF.** Bacterial leakage along the implant-abutment interface of premachined or cast components. Int J Oral Maxillofac Surg 2008;37:177-180.
42. **Nayak AG, Fernandes A, Kulkarni R, Ajantha GS, Lekha K, Nadiger R.** Efficacy of antibacterial sealing gel and O-ring to prevent

micro leakage at implant abutment interface- an in vitro study. J Oral Implantol 2011;May16. (Epub ahead of print).

43. **Oh GJ, Yun KD, Lee KM, Lim HP, Park SW.** Sintering behavior and mechanical porperties of zirconia compacts fabricated by uniaxial press forming. J Adv Prosthodont 2010;2:81-7.
44. **Papavassiliou H, Kourtis S, Katerelou J, Chronopoulos V.** Radiographical evaluation of the gap at the implant-abutment interface. J Esthet Restor Dent 2010;22:235-250.
45. **Pieri F, Aldini NN, Marchetti C, Corinaldesi G**. Influence of implant-abutment interface design on bone and soft tissue levels around immediately placed and restored single-tooth implants: a randomized controlled clinical trial. Int J Oral Maxillofac Implants 2011;26:169-78.
46. **Rack A, Rack T, Stiller M, Riesemeier H, Zabler S, Nelson K.** In vitro synctron-based radiography of microcap formation at the implant-abutment interface of two-piece dental implants. J. Synchrotron Rad 2010;17:289–294.
47. **Ribeiro CG, Maia MLC, Scherrer SS, Cardoso AC, Wiskott HWA.** Resistance of three implant-abutment interfaces to fatigue testing. J Appl Oral Sci 2011;19:413-420
48. **Ricomini Filho AP, de Freitas Fernandez FS, Straioto FG, da Silva WJ,Del Bel Cury AA.** Preload loss and bacterial penetration on

different implant-abutment connection systems. Braz Dent J 2010;21:123-9.

49. **Sharkey S, Kelly A, Houston F, O'Sullivan M, Quinn F, O'Connell B.** A radiographic analysis of implant component misfit. Int J Oral Maxillofac Implants 2011;26:807-815.
50. **Steinebrunner L, Wolfart F, Bössmann K, Kern M.** In vitro evaluation of bacterial leakage along the implant-abutment interface of different implant systems. Int J Oral Maxillofac Implants 2005;20:875-881.
51. **Teixeira W, Ribeiro RF, Sato S, Pedrazzi V**. Microleakage into and from two-stage implants: an in vitro comparative study. Int J Oral Maxillofac Implants 2011;26:56-62.
52. **Tesmer M, Wallet S, Koutouzis T, Lundgren T.** Bacterial colonization of the dental implant fixture-abutment interface: an in vitro study. J Periodontol. 2009;80:1991-7.
53. **Tiossi R, Rodrigues RC, de Mattos Mda G, Ribeiro RF.** Comparative analysis of the fit of 3-unit implant-supported frameworks cast in nickel-chromium and cobalt-chromium alloys and commercially pure titanium after casting, laser welding and simulated porcelain firing. Int J Prosthodont 2008;21:121-123.
54. **Torres JH, Mechali M, Romieu O, Tramini P, Callas S, Cuisinier FJ, Levallois B.** Development of a new quantitative gas permeability method for dental implant-abutment connection tightness assessment. Biomed Eng Online 2011;14;10:28 .

55. **Tsuge T, Hagiwara Y, Matsumura H.** Marginal fit and microgaps of implant-abutment interface with internal anti-rotation configuration. Dent Mater 2008;27:29-34.
56. **Tsuge T, Hagiwara Y.** Influence of lateral –oblique cyclic loading on abutment screw loosening of internal and external hexagon implants. Dent Mater J 2009;28:373-381.
57. **Vasconcellos DK, Bottino MA, Nishioka RS, Valandro LF, da Costa EMW.** The influence of different screw tightening forces on the vertical misfit of implant-supported frameworks. J Appl Oral Sci 2005;13:120-5.
58. **Vigolo P, Fonzi F, Majzoub Z, Cardioli G.** An in vitro evaluation of titanium, zirconia and alumina procera abutments with hexagonal connection. Int J Oral Maxillofac Implants 2006;21:575-580.
59. **Yüzugüllü B, Avci M.** The implant-abutment interface of alumina and zirconia abutments. Clin Implant Dent Relat Res 2008;10:113-21.
60. **Winter W, Möhrle S, Holst S, Karl M.** Bone loading caused by different types of misfits of implant-supported fixed dental prostheses: a three dimensional finite element analysis based on experimental results. Int J Oral Maxillofac Implants 2010;25:947-52.
61. **Zarb GA, Schmitt A**. The longitudinal effectiveness of osseointegrated dental implants in anterior partially edentulous patients. Int J Prosthodont 1993;6:180-188.